INSTITUTO POTOSINO DE INVESTIGACIÓN CIENTÍFICA Y TECNOLÓGICA, A.C.

POSGRADO EN CIENCIAS APLICADAS

Sistemas Finitos Bajo Presión (Finite Systems Under Pressure)

Tesis que presenta

Samuel Eliazar Baltazar Rojas

Para obtener el grado de

Maestro en Ciencias Aplicadas

En la opción de

Materiales Avanzados

Codirectores de la Tesis:

Dr. Aldo Humberto Romero Castro

Dr. Humberto Terrones Maldonado

San Luis Potosí, S.L.P., Julio de 2004.

IPICYT

Instituto Potosino de Investigación Científica y Tecnológica, A.C.

Acta de Examen de Grado

COPIA CERTIFICADA

El Secretario Académico del Instituto Potosino de Investigación Científica y Tecnológica, A.C., certifica que en el Acta 001 del Libro Primero de Actas de Exámenes de Grado del Programa de Maestría en Ciencias Aplicadas en la opción de Nanociencias y Nanotecnología está asentado lo siguiente:

En la ciudad de San Luis Potosí a los 9 días del mes de julio del año 2004, se reunió a las 17:00 horas en las instalaciones del Instituto Potosino de Investigación Científica y Tecnológica, A.C., el Jurado integrado por:

Dr. Humberto Terrones Maldonado	**Presidente**	**IPICYT**
Dr. Mauricio Terrones Maldonado	**Secretario**	**IPICYT**
Dra. Ana Cecilia Noguez Garrido	**Sinodal externo**	**IF-UNAM**
Dr. Aldo Humberto Romero Castro	**Sinodal**	**IPICYT**

a fin de efectuar el examen, que para obtener el Grado de:

MAESTRO EN CIENCIAS APLICADAS
EN LA OPCIÓN DE MATERIALES AVANZADOS

sustentó el C.

Samuel Eliazar Baltazar Rojas

sobre la Tesis intitulada:

Sistemas Finitos Bajo Presión (Finite Systems Under Pressure)

que se desarrolló bajo la dirección de

Dr. Aldo Humberto Romero Castro
Dr. Humberto Terrones Maldonado

El Jurado, después de deliberar, determinó

APROBARLO

Dándose por terminado el acto a las 18:40 horas, procediendo a la firma del Acta los integrantes del Jurado. Dando fé el Secretario Académico del Instituto.

A petición del interesado y para los fines que al mismo convengan, se extiende el presente documento en la ciudad de San Luis Potosí, S.L.P., México, a los 9 días del mes julio de 2004.

Dr. Marcial Bonilla Marín
Secretario Académico

Mtra. Ma. Elisa Lucio Aguilar
Jefa del Departamento de Asuntos Escolares

INSTITUTO POTOSINO DE INVESTIGACIÓN CIENTÍFICA Y TECNOLÓGICA, A.C.
IPICYT
SECRETARIA ACADEMICA

La presente tesis de maestría en ciencias en la especialidad de materiales avanzados fue elaborada por Samuel Baltazar Rojas y aprobada el 09 de 07 de 2004 por los suscritos, designados por el Colegio de Profesores del Departamentode Materiales Avanzados del Instituto Potosino de Investigación Científica y Tecnológica, A. C.

Dr. Aldo Romero C.

Codirector de la tesis

Dr. Humberto Terrones M.

Codirector de la tesis

Dr. Mauricio Terrones M.

Asesor de la tesis

Dra. Cecilia Noguez G.

Asesora de la tesis

La presente tesis de Maestría en Ciencias Aplicadas opción Materiales Avanzados fue elaborada por el Fis. Samuel Eliazar Baltazar Rojas y aprobada el 16 de junio de 2004 por los suscritos designados por el Colegio de Profesores del Departamento de Materiales Avanzados del Instituto Potosino de Investigación Científica y Tecnológica, A.C.

Dr. Humberto Terrones Maldonado
Co-director de tesis

Dr. Aldo Humberto Romero Castro
Co-director de tesis

Dr. Mauricio Terrones Maldonado
Comité Tutoral Interno

Esta tesis fue elaborada en el Departamento de Materiales Avanzados para la Tecnología Moderna del Instituto Potosino de Investigación Científica y Tecnológica, A. C., bajo la codirección de los doctores Aldo Romero C. y Humberto Terrones M.
Durante la realización del trabajo, el autor recibió una beca académica del Instituto Potosino de Investigación Científica y Tecnológica, A. C. asi como del apoyo dado por Consejo Nacional de Ciencia y Tecnología a los proyectos: W-8001 (HT,MT,AHR) iniciativa Millenium, G2585-E(HT,MT), 36365-E(HT), 37589(MT) y UCMEXUS (California University).

Thesis Committee

Advisor Members :

Dr. Aldo Romero C.

Advanced Materials, IPICYT

Dr. Humberto Terrones M.

Advanced Materials, IPICYT

Local Member :

Dr. Mauricio Terrones M.

Advanced Materials, IPICYT

External Member :

Dra. Cecilia Noguez G.

Instituto de Física, UNAM

Sistemas finitos bajo presión

Samuel Baltazar Rojas

Tesis para optar al grado de Maestro en Ciencias Aplicadas

Junio, 2004

Resumen

El estudio de estructuras bajo condiciones extremas como altas presiones, puede entregarnos nuevas configuraciones y/o situaciones que son metaestables bajo condiciones normales. Estas transiciones pueden estar asociadas a nuevas propiedades electrónicas y mecánicas.

En este trabajo se discuten diversos métodos teóricos para estudiar sistemas finitos bajo presión en un marco clásico. Se han implementado algunos métodos ya publicados y se comparan con dos nuevas definiciones propuestas en este trabajo. Además se han comparado las predicciones de cada uno de ellos aplicados a diferentes sistemas físicos. Los métodos pueden ser divididos en dos grupos principales; el primero depende de una extensión del término termodinámico PV mientras que en el segundo el sistema finito es incluido en un reservorio de presión.

Junto con discutir la importancia del volumen asociado, se han considerado diversos sistemas finitos para comparar los métodos. Transiciones estructurales en nanotubos de carbono, nanodiamantes y clusters metálicos son presentados en este trabajo y su comportamiento como función de la presión externa son discutidos.

Finite systems under pressure

Samuel Baltazar Rojas

Submitted for the degree of Master in Applied Sciences

June, 2004

Summary

The study of systems under extreme conditions like high pressures can give us novel structures and/or configurations that are metastables under normal conditions. These transitions could be associated to new electronical and mechanical properties. In this work we discuss several theoretical methods to simulate finite systems under pressure. We have implemented techniques already published and compared with two new methods proposed by us. We compare the predictions of every one of them and present results on different physical systems. The methods can be divided in two main groups, one which depends on an extension of the thermodynamical term "PV" and the second one which is the simulation of a finite system embedded in a pressure reservoir. In general, we have implemented five different volume defintions: an atomic volume representation, an average description of cluster volume, a volume definition from gyration radii, the Quick Hull volume definition and an a volume defined from surface coordinates. We discuss the importance of a good volume definition. Our results show the fullerene C_{60} molecule collapses at pressures around 35-40 GPa. The study of single walled carbon nanotubes (SWCNTs) and gold clusters reveals that the adapted convex volume definition is more suitable to describe hollow systems, and that the volume definition considering a gyration radii can be applied to compacted structures such as metallic clusters. Bond transitions of carbon nanotubes, nanodiamond and onion structures are also described. For cubeoctahedral gold clusters, we observed structural changes at pressures larger than 10 GPa at 300 K.

Acknowledgments

I would like to express my thankful to my advisors, Dr. Aldo Humberto Romero due to its numerous advices, my innumerable visits every day to his office that helped to me to finish this work on time, and also Dr. Humberto Terrones M., in particular several aspects of the results presented in these work has been enlighted by his discussions. I also would like to express my gratefully to Dr. Jose Luis Rodríguez-López for his contribution, specially in the study of metallic clusters.

I am also grateful for the structural coordiantes used in this work to Dr. Mauricio Terrones M., Dr. Humberto Terrones., Dr. Jose Luis Rodríguez-López and Dr. Aldo H. Romero. At this point, I would like to thank the support given to me from my classmates and the rest of the Advanced Materials Department (researchers and technicians).

I would like to thank to my family, whose in spite of the distance, always have given to me their best wishes.

In conclusion, I would like to express my gratitude to the Institute for Scientific and Technological Research of San Luis Potosí (IPICYT), for the financial assistance and I recognize the support given by grants from CONACY: W-8001 Millenium initiative(HT,MT,AHR), G2585-E(HT,MT), 36365-E(HT),37589(MT) and UCMEXUS (California University).

Dedicated to my parents
Camilo and Juana,
and all my family

Contents

List of Tables

List of Figures

Chapter 1

Introduction

1.1 The need for computational simulations

Characterisation, description and detailed studies on materials were developed considering, three main streams: experimental work, the analytical solution of simple or more elaborated models and by making mechanical simulations.

The experimental work designed to solve a problem can be, in many cases, easily performed or implemented for a single case, but it would be difficult to study the given system as function of different parameters. For example, the characterisation of the physical transitions such as the boiling or freezing points of water at atmospheric pressure were studied long ago [1]. If our interest is to study this behaviour as function of pressure, we certainly have to face new challenges to design the experiment; how we can get the properties that are desirable to know in the less expensive way.

A second approach to study physical systems has been derived from proposing simple models which can be solved analytically or using perturbation theory. Even though, this approach is still very important in physics, the complexity of the systems we have to study nowadays restrict its applications. Starting with simple laws such as Newton's laws, it is possible to predict the whole dynamical behaviour but with the difficulty of solving the equations of motion as the number of degrees of freedom increase. The main difficulty with this approach comes from two different views, on one hand, the potential interactions among atoms have to be defined as

simple as possible, such that the equations of motion can be solved; and in the other hand, the electronical properties become important and the problem enters into the quantum mechanics regime.

The last chosen possibility known before the computer era, was based on the study of systems by a simple macroscopical model which shows the same searched behaviour. As an example we can mention the study of dense liquids. It was systematically developed by *J.D. Bernal* [2, 3], considering large ensembles of spheres arranged such that the dynamical behaviour mimics the behaviour of atoms in a liquid. The enormous effort that was necessary to design these simulations and subsequent analysis (for example to characterise local package geometries) shows the importance to solve these problems using computers as soon as they were available for researchers.

1.2 Motivation

The field of computational physics allows us to study physical phenomena that before the appearance of computers were difficult to solve before computers appeared. In spite of analytical solutions which provide the exact information and detail on time and length scales, computational methods allow us to predict with large precision and some times using a more accurate model (even though usually more complex), physico-chemical properties of a molecule, crystalline systems, liquids, etc.

Computational physics becomes a bridge between experimental work and the efforts of theoreticians. Simulations are used to reproduce and predict experimental observations, or at least to obtain qualitative behaviours found in the experiment. These techniques are also able to implement a *virtual laboratory* that allows us to discover novel material properties under conditions that have not been observed in the experiment. For example, some of the first works of liquid transitions were developed by *Alder and Wainwright*, who found a first-order freezing transition of a liquid system [4] before that experiments were carried out. By implementing different force fields between the atoms, they were able to conclude that repulsion

forces instead of attractive interactions are dominant for this transition (result that is relevant in the work present in this thesis). It can be found many other examples where computational methods are able to compare, predict or explain some of the most important experimental observations over the last decades.

Here we focus on the characterisation of finite systems under hydrostatic pressure. The study of those systems such as clusters, nanocrystals, biological systems, has important implications in astrophysics, geophysics, biology, chemistry, electronics ,etc [5–7]. Although there is a large number of experimental examples (the systems now known as nanostructures fall into this category), the theoretical part has been rather superficial. Among many experimental studies, one who has attracted a large interest is the structural characterisation of clusters, metallic nanoparticles or carbon nano-systems, molecular systems, etc. structural changes on these nanostructures result in significant variations in the electronic, optical and transport properties.

The development of theoretical methods such as extended Lagrangian (see chapter 2), has opened different routes to simulate physical systems of different ensembles. Those methods have been implemented considering ion interactions (classical methods), electronical properties (quantum-mechanical methods). In the case of applied hydrostatic pressure at constant temperature, there are two main methods that have been used since the 80's: constant-pressure molecular dynamics proposed by *Andersen* [8] and an extension given by *Parrinello-Rahman* [9]. Various examples are found in the literature, where the agreement between experimental observations and theoretical predictions under these methods have been recognised. Unfortunately, these methods have only been developed for infinite systems (periodicity condition in crystals).

Studies of finite systems using a classical mechanic or a quantum mechanical apporach have no been fully developed. It is clear that a more accurate method should consider quantum mechanics in their description and therefore only first principle calculations appear more suitable to explain any physical observation. In this context, we are restricted to study a reduced number of atoms due to the large computational effort required. Consequently, the classical methods are still of great

advantage when a large amount of calculations or atoms have to be considered. In such a case, the potential energy used to represent atom interactions are taken from a more accurate calculation or from a parametrisation of functional interactions, in which these parameters are obtained by combining observables and experimental measurements.

In this work we are interested in studying finite, non-periodic systems, under hydrostatic pressure. The change of this variable (pressure) could lead to structural transformations, or to rearrangements of the atomic positions so that the total energy of the system decreases. We believed, that these types of simulations could be helpful in the experimental work. Even though, the methods for simulating systems under pressure are well known since the 80's, none of these can be applied directly to a finite system. More recent implementations are based on applying the pressure to a box where the system is embedded and where the periodic images are included. In the case of a finite system, there is not such a periodicity and there is no physical meaning for a box enclosing such a system. Only recently, some reports have performed calculations a long these lines using an extended Lagrangian for finite systems [10,11]. They have been applied to Al_n clusters [12], carbon nanotubes [10], graphite [11] and metal nanoparticles [13]. An additional term included in the Lagrangian is based on a well-defined volume for finite systems. This is a critical issue, mainly because this quantity cannot be defined uniquely. On the other hand, a more general thermodynamical model has been also presented very recently by *Martonak et al.* [14]. This method assumes that a finite system is embedded in a fluid of classical and repulsive particles which provide pressure as function of the particle interactions, temperature and volume which encloses the two systems (fluid and cluster). They have applied this method to many different system, finding important structural changes due to the applied pressure.

Therefore, we present and discuss all different methods known until now, which are able to simulate finite systems under pressure. Even though, the methods we discuss here are going to be applied to systems where we assume a classical interaction, these methods can be easily generalised considering quantum mechanical approaches. In the theoretical presentation, we also propose different methods in

order to apply different methodologies to several important finite systems such as fullerenes (C_{60}), carbon nanotubes concentric fullerenes, carbon nanodiamonds and metallic clusters.

1.3 Thesis objectives

In this work we accomplish each one of the following goals:

- To implement computational algorithms which solve the equation of motion for atoms considering different models for simulating systems under hydrostatic pressure. Besides those already proposed in the literature, we suggest new methods and we show that our methods are in agreement with a method proposed by *Martonak et al.* [14] and based in a tight-binding approach and experimental observations. The program language chosen is **FORTRAN 90**. In order to analyse the results obtained in our simulations, we used different packages such as **Cerius^2, xmgrace, SYMMOL, MOLEKEL**, or we created necessary routines to perform specific analysis.

- To compare and analyse the results of the dynamical atomic trajectories obtained from different methods for a C_{60} fullerene, carbon nanotubes and nanodiamonds. Based on these results, we select a suitable model to apply an external pressure considering other systems.

- To study nanodiamond structures under hydrostatic pressure and temperature trying to find structural transitions of these nanoparticles and eventually to compare with experimental results available in the literature.

- To study single walled carbon nanotubes under hydrostatic pressure and temperature in order to search for structural transitions, and compare the results with published data.

- To study concentric fullerene structures (sometimes called graphitic *onions*) under pressure at different temperatures in order to find structural transformations from concentric fullerenes to diamond structures or amorphous phases.

- Study of metallic systems (gold clusters) under pressure and find structural transitions that have been detected in previous experimental works.

1.4 Overview

The chapter 2 provides a theoretical framework defining the isobaric-isothermal ensemble that has been considered in our work. Subsequently, we describe the atomic interaction potentials that are used to model the different nanostructures: Tersoff-Brenner potential applied to covalent systems and the Gupta potential applied to metallic systems.

The volume is an important factor and we present five definitions of a finite system that will be applied to various structures. In addition, an additional method that doesn't need to consider the volume of the cluster to apply an external pressure, is modified from a previous work by Martonak et al.

Chapter 3 shows the scheme of the algorithms developed in this work and some routines implemented in order to obtain the equations of motion. On chapter 4, we consider the results obtained from our simulations applied to numerous finite systems and finally on the chapter 5, the main conclusions of our work and the future research are presented.

Chapter 2

Theoretical background

2.1 Extended Lagrange methods

From theoretical physics is well known that the Lagrangian (or Hamiltonian) is the functional which contains the complete representation of a given system, as long as the potential energy is well defined. If we now start from the general Lagrangian functional, an external pressure can be added to the system if we follow a similar approach as in thermodynamics. The pressure is defined as the change of energy as function of volume, therefore volume becomes an adjustable variable function. Now, when a pressure is applied to any system, the enclosed volume changes until the internal pressure balances out the applied external pressure. The way to include this observation in the equations, it is by adding a term like a pressure with its conjugate variable, *the volume*, so that the Lagrangian is now expressed as

$$\mathcal{L} = \sum_{i}^{N} \frac{p_i^2}{2m_i} - (\phi(\{r_i\}) + P_{ext}V) \tag{2.1}$$

where r_i, m_i and p_i are coordinates, mass and conjugate momentum of each atom i ($i = 1, \ldots, N$) respectively, ϕ is the particle interaction potential and V corresponds to the volume occupied by the system particles.

The equations of motion could derive from equations:

$$\frac{\mathrm{d}}{\mathrm{d}t}\left(\frac{\partial \mathcal{L}}{\partial \dot{r}_i}\right) = \frac{\partial \mathcal{L}}{\partial r_i} \tag{2.2}$$

and applying the previous equations to the Lagrangian (eq. 2.1), we obtain the equations of motion for every particle position as

$$m_i \frac{\partial^2 r_{i,\alpha}}{\partial t^2} = F_{i,\alpha} - P_{ext} \frac{\partial V}{\partial r_{i,\alpha}} \qquad \alpha = x, y, z; \quad i = 1, \ldots, N \tag{2.3}$$

These equations describe a set of particles interacting via a conservative force (derived from the potential ϕ) and an applied external pressure, a constant pressure canonical ensemble. Letting the system evolving up to equilibrium, the average change of the virial quantity ($\sum \mathbf{r} \cdot \mathbf{p}$ where $\mathbf{r}$ and $\mathbf{p}$ are the position and momenta vectors) respect to time is zero [15], giving an expression

$$\langle \Big(\sum_i^N m_i v_i^2 - \sum_i^N \mathbf{r}_i \cdot \nabla\phi - \sum_i^N \mathbf{r}_i \cdot P_{ext} \nabla V \Big) \rangle = 0 \tag{2.4}$$

and then

$$\langle \sum_i^N m_i v_i^2 - \sum_i^N \mathbf{r}_i \cdot \nabla\phi \rangle = \langle \sum_i^N \mathbf{r}_i \cdot P_{ext} \nabla V \rangle \tag{2.5}$$

If the volume is a parametric function of the atomic coordinates of degree 3 ($V(\lambda r_i) = \lambda^3 V(r_i)$), we could apply Euler's theorem, which for this particular case takes the form:

$$\sum_i^N \mathbf{r}_i \cdot \nabla_i V = 3V \tag{2.6}$$

By replacing eq. 2.6 into eq. 2.5, we obtain

$$P_{ext} = P_{int} = \langle \frac{1}{3V} \Big(\sum_i^N m_i v_i^2 - \sum_i^N \mathbf{r}_i \cdot \nabla\phi \Big) \rangle \tag{2.7}$$

which corresponds to the pressure version of the virial theorem. The internal pressure P_{int} balances out the applied external pressure. It is noteworthy that the internal pressure depends directly on the interparticle potential, but more importantly on the volume, thus indicating that the volume definition is **critical** to ensure that the virial theorem applies.

We now start describing the interaction potentials used in this work, followed with a discussion of several volume definitions, some of them have been published and others came from our extensions. As a comparison, we have also performed an implementation of a different approach, which considers a cluster in contact with a liquid bath, which serves as a pressure reservoir [14]. Even though, this method is

not really the core of the present work, we use this method as a ground comparison, mainly because this method can be proved to give a proper description of finite systems under pressure [22].

2.2 Potential interaction definitions

In this work we have focused in two different types of systems; covalent and metallic monoatomic particles. In particular, we have implemented classical potentials for carbon and gold atoms. By defining the interparticle potential interaction in each case, we could proceed by solving the equations of motion of a given finite system under pressure. Every one of the potentials have been throughly tested by other authors and they have been used extensively to calculate many different crystalline and liquid properties. In the case of the carbon, the interparticle potential is a three body potential, which has been successfully applied to crystalline carbon and silicon systems [16] and adapted to study fullerene structures [17]. In particular, we have followed the implementation considered by Maruyama et al [18] to study fullerene formation.

On the other hand, we have used the semiempirical Gupta potential in order to model interactions between metallic atoms [19]. This potential has been obtained by using the tight-binding second moment approximation as it is summarized below.

2.2.1 Tersoff-Brenner potential for covalent systems (carbon)

The energy of carbon systems can be described as the sum of many body interactions between all carbon atoms in a given system, which is reduced to a three body interaction in the Tersoff-Brenner aproximations as:

$$U = \sum_i \sum_{j(j>i)} [V_R(r_{ij}) - B^*_{ij} V_A(r_{ij})] \tag{2.8}$$

where r_{ij} is the carbon-carbon distance and the repulsion (V_R) and attraction (V_A) terms are:

$$V_R(r) = f(r)\frac{D_e}{S-1}\exp\{-\beta\sqrt{2S}(r-R_e)\} \tag{2.9}$$

$$V_A(r) = f(r)\frac{D_e S}{S-1}\exp\left\{-\beta\sqrt{\frac{2}{S}}(r-R_e)\right\} \tag{2.10}$$

where the cutoff function is defined as:

$$f(r) = \begin{cases} 1 & (r < R_1) \\ \frac{1}{2}\left(1 + \cos\frac{r-R_1}{R_2-R_1}\pi\right) & (R_1 < r < R_2) \\ 0 & (r > R_2) \end{cases} \tag{2.11}$$

The many-body coupling is represented by B^*_{ij}, that is angular dependent bonds $i-j$ and $i-k$ produced by the local environment of atom i.

$$B^*_{ij} = \frac{B_{ij} + B_{ji}}{2} \quad \text{with} \quad B_{ij} = \left(1 + \sum_{k(\neq i,j)} \Big[G_c(\theta_{ijk}) f(r_{ik})\Big]\right)^{-\delta} \tag{2.12}$$

where:

$$G_c(\theta) = a_0\left(1 + \frac{{c_0}^2}{{d_0}^2} - \frac{{c_0}^2}{{d_0}^2 + (1+\cos\theta)^2}\right) \tag{2.13}$$

Figure 2.1 shows a schematic representation of interactions considered in the Tersoff-Brenner potential used in this work. The three body potential appears as function of an angle formed by 3 carbon atoms and it is usually called *bond-angle*. Table

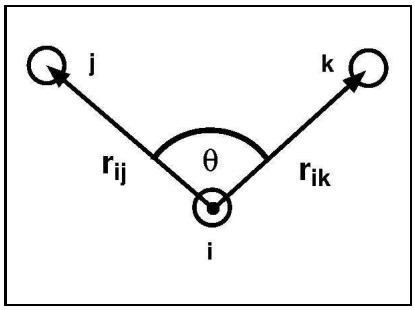

Figure 2.1: Three-body interaction model.

2.1 presents the parameters fitted by Maruyama et al [18], which are the ones used in this work. These parameters were modified from the original Tersoff-Brenner definitions [20] and applied to study properties of fullerenes and single-walled nanotubes (SWNTs).

Using the fitted parameters in this model, we study carbon structures such as shown in Fig. 2.2. Note that we have also included structures where Van der Waals interaction play an important role at equilibrium conditions. These interactions are less important when an external pressure is applied to the system. Fig. 2.2(a) corresponds to a model of carbon cluster diamond-like (293 atoms) with sp^3 hibridized

Table 2.1: Carbon Parameters

Parameters	D_e [eV]	S	β $[\mathring{A}^{-1}]$	R_e $[\mathring{A}]$	R_1 $[\mathring{A}]$	R_2 $[\mathring{A}]$	δ	a_0	c_0	d_0
Carbon	6.00	1.22	2.10	1.39	1.70	2.00	0.50	$208.13 \cdot 10^{-6}$	330.00	3.50

carbon atoms inside the shell and sp^2 and sp carbons on the surface. the model shown in Fig. 2.2(b) is an example of concentric carbon cages of three layers (800 atoms corresponding to $C_{60}@C_{240}@C_{500}$) and Fig. 2.2(c) is a fullerite cluster taken from an fcc structure (780 atoms).

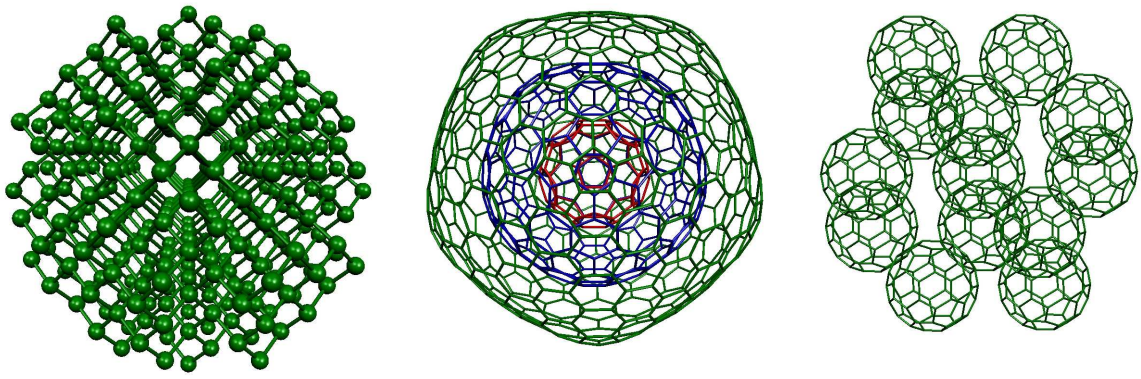

(a) (b) (c)

Figure 2.2: Carbon structures:(a) Nanodiamond, (b) Structure type graphitic onion and (c) fullerite cell.

2.2.2 Gupta potential for metallic systems

The study of transition metal clusters and metallic alloys has been widely developed both theoretically and experimentally [13, 37, 47]. Among different theoretical approaches, the one which has received a lot of attention, due to its good agreement with experimental observations, is a classical many-body molecular dynamics; providing a good representation of crystalline phases and clusters structures. This potential has also described more-or-less accurately elastic properties, diffusion dynamics, thermal transport coefficients,etc. In this context, the bond interatomic potential describes the interaction as a function of the interatomic distance of all particles (up to a cutoff).

The Gupta potential considers two terms: i) a **hopping integral or overlap term** and ii) an **ionic repulsion term**:

$$E_c = \sum_i (E_R^i + E_B^i) \tag{2.14}$$

where E_c is the total binding energy obtained as individual contributions of terms

$$E_B^i = -\Big[\sum_j \xi_{\alpha\beta}^2 e^{-2q_{\alpha\beta}(r_{ij}/r_o^{\alpha\beta}-1)}\Big]^{1/2} \tag{2.15}$$

$$E_R^i = \sum_j A_{\alpha\beta} e^{-p_{\alpha\beta}(r_{ij}/r_o^{\alpha\beta}-1)} \tag{2.16}$$

where E_B^i and E_R^i are the binding and repulsion terms respectively.

This model has been obtained by Gupta by using tight-binding calculations [24]. In this work, we have extracted the different optimized parameters used for this potential from a previous work reported by Cleri and Rosato [19], who generated a table of parameters for several transition metals and tested the potential for different atomic structures and environments. These parameters have been obtained for Ni, Cu, Rh, Au, Pb, etc. In this work, we focus on monoatomic metallic systems specifically Au, where many papers have been published testing its agreements with experimental conditions [62–64]. We also would like to identify the stability of the cluster symmetry as function of pressure and possible structural transformations. Typical nanoclusters that we have considered in this work are shown in Fig 2.3 a-b.

Table 2.2: **Gold parameters**

Metal	A[eV]	ξ [eV]	p	q
Au	0.2061	1.790	10.229	4.036

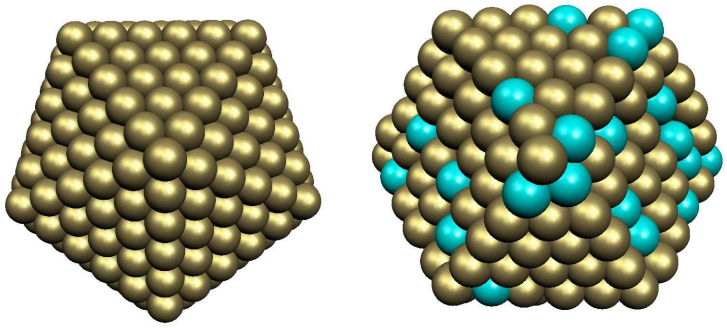

(a) (b)

Figure 2.3: Metallic Clusters.(a) shows a cluster of Au with Icosahedral symmetry and (b) corresponds to an Octahedral symmetry of an alloy Au-Cu

2.3 Functional volume definitions

In order to perform a complete assessment on the functional form of the volume as a function of the atomic coordinates, we have implemented five different possible definitions. Three of them have been reported already in the literature and two of them are basically our own contribution. The definitions can be divided in two main groups. A first group is a volume function which depends on all atomic coordinates of the finite system of interest. Usually, the volume formula makes an estimation of the real enclosed volume. The benefit of using these functional forms is that they are continuous and the partial derivate can be exactly calculated; they are involved directly in the equations of motion of every particle and make the method rather efficient. The second group corresponds to define the volume of the system by using the surface particles which are only on the surface. This method is more precise but it has the difficulty that the atoms that belong to the surface have to be identified

on each iteration.

From the first volume group, we have considered three different volume definitions: (a) atomic volumes (applied to Ni nanocrystals and carbon nanotubes) [10], (b) average interparticle distance [11] and (c) radii of gyration volume, which was proposed previously but never implemented in the past, it was used only to calculate a postprocessing analysis of Al_n clusters [12].

From the second volume group, we have considered two different volume definitions. A first one which has been recently implemented [13] and basically estimates the volume from a convex volume (a minimal polyhedron that encloses the structure) using the QuickHull algorithm (see below) [30]. This volume, is an overestimation of the real volume in cases where the structure is concave. It was implemented on MonteCarlo simulations, and the goal was to minimize the energy with the extra VP term but no dynamical evolution was studied. Here we have done a similar implementation but including the PV term on the dynamical equations of motion only for the surface belonging to the enclosing polyhedron. The last volume definition we have used in this work starts from calculating a triangular surface (also called Delaunay triangulation) which encloses tightly the structure. This is an extension of the previous definition but here the volume is able to cover (to some extend) concave parts if they are present on the structure.

The major difference between algorithms used for periodic and non-periodic systems is the use of ficticious variables. These kind of variables, ficticious kinetic energy and ficticious mass, are coupled to the cell variables in periodic systems, which are added to the Lagrangian. In order to avoid kinetic energy transfer between the cell and clusters, we have to consider appropriated values to these variables, as well as the time step has to be the largest value to perform a simulation.

2.3.1 Total coordinates Dependence

The atomic volume representation (Type I)

As it was discussed previously, in order to have a precise simulation method by using the PV term extension in the Hamiltonian, it is critical to have a proper

volume definition. The first approach in this direction was presented by *Sun* and *Gong* [10]. The definition depends on all atomic positions and there is not an adjustable parameter. The volume is represented as the sum of independent terms which are atomic volumes

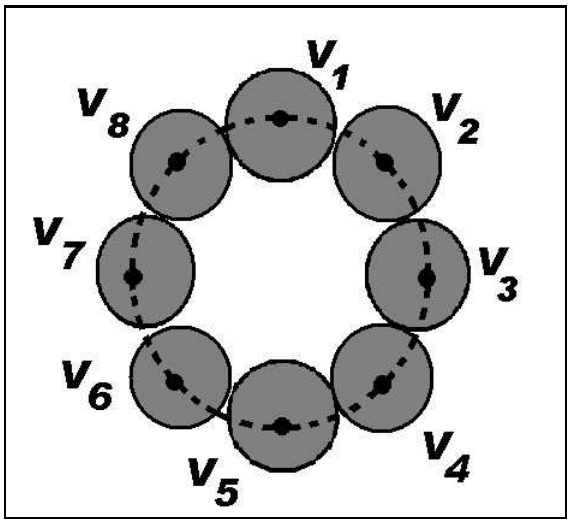

Figure 2.4: First volume definition considering the atomic volumes.

$$V = \sum_{i}^{N} V_i \tag{2.17}$$

where each atomic volume V_i is represented by a cubic function

$$V_i = \sum_{j \neq i} f(r_{ij}^3) \tag{2.18}$$

This volume definition is based on the well known definition of the Wigner-Seitz primitive cell. We obtain the individual volumes using a scaled volume of independent atomic spheres (a schematic view is shown in Fig. 2.4)

$$V_i = \gamma_i \frac{4\pi}{3} \sum_{j \neq i} \left(\frac{r_{ij}}{2}\right)^3 \tag{2.19}$$

where the sum is made over nearest neighbours and γ_i is a scale factor that is the inverse of nearest neighbours number of each atom i.

Using this definition we have calculated volume variations with respect to atoms and coordinates; giving

$$\frac{\partial V}{\partial r_{i,\alpha}} = \frac{\pi}{2}\gamma_i \sum_{j \neq i} r_{ij} \cdot (r_{i,\alpha} - r_{j,\alpha}) \qquad \alpha = x, y, z \tag{2.20}$$

where $r_{i,\alpha}$ is the α-component of $\vec{r_i}$ and $r_{j,\alpha}$ corresponds to the α-component of $\vec{r_j}$. This expression was introduced in the equations of motion for every particle 2.3. It is noteworthy that external pressure affects the position of every particle but it does it only through changes of atomic local volumes.

It is important also to note that this definition is very simple to implement but it is a very crude estimation of the real volume. Therefore, the actual pressure could be overestimated as we show in chapter 4. Besides, the estimation of the volume from atomic volumes could be more appropriate to compact structures; in cage-like structures, this definition becomes very unrealistic and could lead to wrong results.

The average interparticle description of cluster volume (Type II)

A more adequate volume definition could arise from the observation that the volume scales as a spherical length scale $V \sim R^3$ as was proposed by Landau [11]. He defines the volume using this scaling form and taking R as the average interparticle distance (see Fig. 2.5). The cluster is then mapped to a spherical shape with a radius equal to the average particle distance. The distance between atom i and atom j is defined as follows

$$r_{ij} = \Big[\sum_{\alpha}(r_{i,\alpha} - r_{j,\alpha})^2\Big]^{1/2} \qquad \alpha = x, y, z \tag{2.21}$$

and the atomic average distance is given by

$$R = \Big(\frac{1}{N(N-1)} \sum_{i=1,j=1}^{N} \big[\sum_{\alpha}(r_{i,\alpha} - r_{j,\alpha})^2\big]\Big)^{1/2} \tag{2.22}$$

In the functional form introduced in ref. [11], an initial volume is scaled through the changes of the interparticle distance to provide the volume variation over time as

$$V = V_{ini}\frac{R^3}{R_{ini}^3} \tag{2.23}$$

where R_{ini} and V_{ini} are the initial average distance and the initial volume respectively. These values could be obtained by atomic initial positions and evaluating the

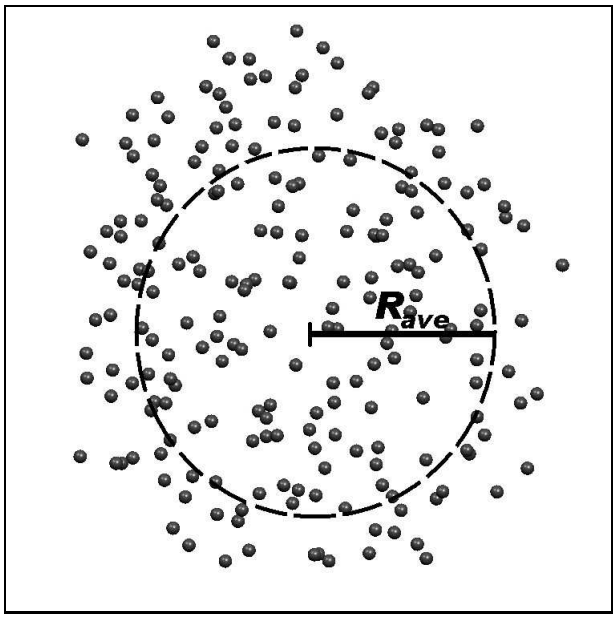

Figure 2.5: Example of a volume cluster according to the average interparticle description.

volume using any definition. For example; atomic volume (see previous section) or volume from gyration radii (defined in the following section) are considered in order to stablish an initial volume.

As we have mentioned before, we need to consider variations of volume due to changes in their atomic positions to be included in the particle equations of motion. These terms could be obtained as

$$\frac{\partial V}{\partial r_{i,\alpha}} = \frac{V_{ini}}{R_{ini}^3} \frac{3R}{N(N-1)} \sum_{j \neq i}^{N} (r_{i,\alpha} - r_{j,\alpha}) \tag{2.24}$$

The volume from gyration radii (Type III)

Another functional volume we could choose (as previously suggested in Ref. [12]), it is to define the volume from the radii of gyration R_i (see Fig. 2.6). Thus R_i is defined as

$$R_i = \sqrt{I_i/N} \tag{2.25}$$

where I_i corresponds to principal inertial moments of the system and M is the total mass. The cluster volume can be approximated by

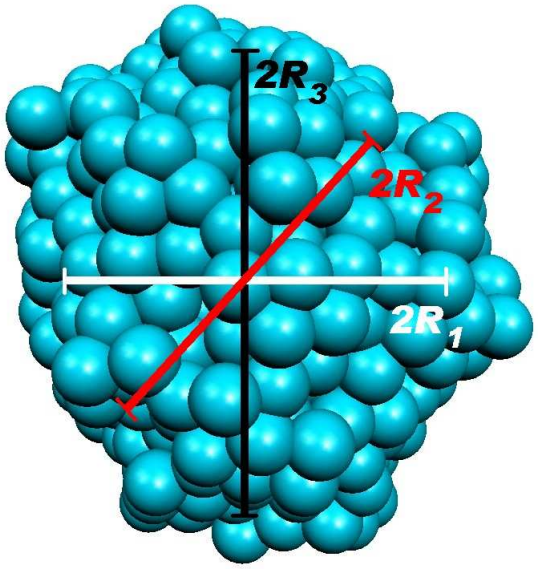

Figure 2.6: Gyration radii used to define the volume of a cluster. They are along the principal axis.

$$V \approx \frac{4}{3}\pi R_1 R_2 R_3 \tag{2.26}$$

An evaluation of these quantities requires to calculate the inertia tensor (a symmetric matrix), which is defined as

$$I = \begin{pmatrix} I_{xx} & I_{xy} & I_{xz} \\ I_{yx} & I_{yy} & I_{yz} \\ I_{zx} & I_{zy} & I_{zz} \end{pmatrix} \tag{2.27}$$

where each one of these terms are

$$I_{jk} = \sum_i m_i (r_i^2 \delta_{jk} - x_{i,j} x_{i,k}) \tag{2.28}$$

As it is known, the trace of a matrix is invariant under unitary transformations, therefore, the quantity that matters is the determinant of this tensor as

$$det(I) = -I_{xz}^2 I_{yy} + 2I_{xy} I_{xz} I_{yz} - I_{xx} I_{yz}^2 - I_{xy}^2 I_{zz} + I_{xx} I_{yy} I_{zz} \tag{2.29}$$

Finally the radii or gyration volume definition can be expressed by

$$V = \frac{4}{3}\pi \sqrt{\frac{I_1 I_2 I_3}{N^3}} = \frac{4}{3}\pi \sqrt{\frac{det(I)}{N^3}} \tag{2.30}$$

As discussed earlier, this definition depends on all system coordinates, and the volume variations affect each equation of motion. In order to evaluate variations of volume for every particle and coordinate we could use

$$\frac{\partial V}{\partial r_{i,\alpha}} = \frac{1}{2VN^3}\left(\frac{4}{3}\pi\right)^2 \frac{\partial det(I)}{\partial r_{i,\alpha}} \tag{2.31}$$

This definition is quite accurate describing cage-like structures as well as compact structures but the real volume is always underestimated by a 20-30%. This will affect the real pressures required to produce changes on the system. The benefit of using this definition, it is that the pressure is included directly in the equations of motion and makes the implementation quite efficient when compare to other definitions.

2.3.2 Volume from surface coordinates

The second group of volume definitions that we have considered takes into account a volume enclosed by a surface. It is clear that the real volume of a system is really described *only* by the surface atoms (see below).

The Quick Hull volume definition (Type IV)

A simple method to estimate the volume enclosed by a surface is the one defined through the convex volume (applied to metallic systems by Calvo et al [13]). This method calculates the minimal convex polyhedron that encloses the structure. First of all, an identification of the surface atoms has to be performed, which are the planes which form the convex polyhedron as shown in Fig. 2.7. The planes defined from this polyhedron enclosed completely the volume of the cluster. The Quickhull algorithm is a very fast method to calculate the smallest convex polyhedra that encloses a point set P (for additional details we refer the reader to ref. [30]). This algorithm is able to identify a set of planes which form a polyhedron. A major failure in describing a structure, it is that coplanar particles or concave structures do not belong to the surface. In our implementation, this observation has an important consequence, the pressure can only be applied to atoms on the plane vertexes found in the search of the polyhedron. Although these points are not considered,

the volume of the structure is very precise and quite accurate in most of the systems we have considered in this work. Below, we will discuss the cases where this implementation can give wrong results.

After the polyhedron has been found, the unitary vectors perpendicular to every

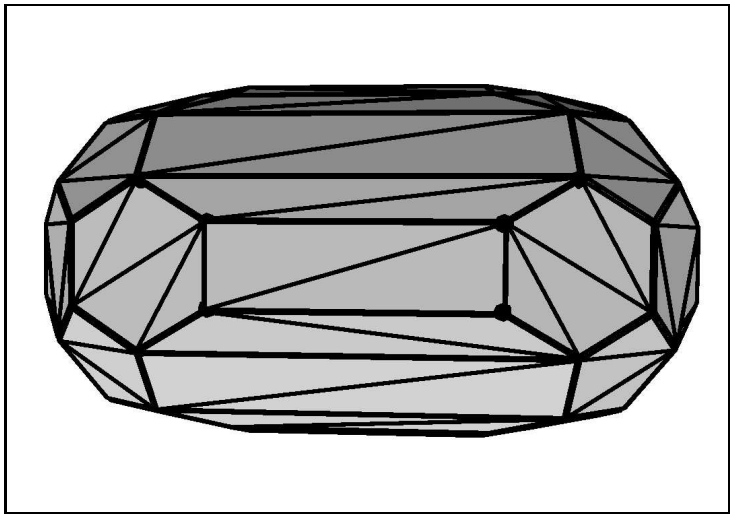

Figure 2.7: Vertexes of single walled carbon nanotubes are used to generate areas and the volume approximation.

face has to be calculated. We assume that pressure is completely hydrostatic (perpendicular to the surface) and every face will feel the pressure proportional to the area. After the unit vector has been found, we take the pressure as a force perpendicular to the face ($F_i^{ext} = P \cdot A_i$ where A_i correspond to the area) and it is applied to every vertex by taking the pressure, multiplying it by the area and distributing the force to each vertex ($F_{i,\alpha}^{ext} = F_i^{ext}/N$, where N is the number of vertexes of a given plane). This method only affects the motion equation particles, which belong to the convex hull surface as follows

$$m_i \frac{\partial^2 r_{i,\alpha}}{\partial t^2} = F_{i,\alpha} - F_{i,\alpha}^{ext} \qquad \alpha = x, y, z; \quad i = 1, \ldots, N \tag{2.32}$$

where N corresponds to the effective number of vertexes (N $\leq$ number of atoms on the surface).

This method is not as efficient as those described earlier. Here, the evaluation of the volume and the search of the surface atoms has to be performed for every iteration. The volume is usually as 90-100% close to the real volume, if the structure does not

possess concavities.

The adapted convex volume definition (Type V)

As described in the previous section, the use of an extended Lagrangian in simulating finite systems under pressure, it is based on having a good volume description of the structure. The best volume defined until now it is based on the convex hull algorithm (see previous section) but it fails to describe structures with concave geometries. Here we generalise the convex hull method by relaxing the search of the atoms on the surface and describing them by a triangulation which encloses tightly the structure.

In this generalisation, the algorithm could be described as follows:

- For every atom i, all triangles containing the atom and two other neighbours (up to a given cutoff) are calculated, they are defined through a plane which contains all three points. We discard all triangles that are inside the structure and we called those as *interior planes*. For example, for a given plane ($Ax + By + Cz + d = 0$), we consider all particle positions (x_A, y_A, z_A) within the enclosed region (inside the given cutoff) and evaluate the plane equation on every one of those atomic coordinates as follows $Ax_A + By_A + Cz_A + d = \delta$, the plane is discarded if $\delta \geq \epsilon$ for any of the coordinates considered, where ϵ is a tolerance parameter.

- Considering all remaining planes, the algorithm neglects planes with a normal vector directed towards the interior of the structure. Also the triangles that contain another triangle are deleted.

- At this step, all surface triangles that intersect its area with another previously considered are deleted.

- Finally, the areas, normal vectors and vertexes associated to each remaining triangle and volume of the structure are calculated.

An example of this algorithm applied to a structure (the same system used in previous section) is shown in Fig. 2.8. The external pressure is applied to the system

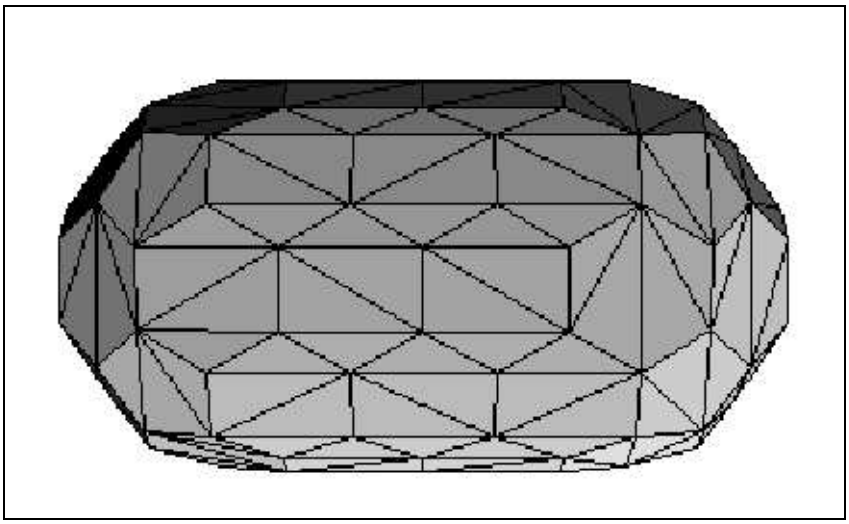

Figure 2.8: The same SWCNT is used in Fig.2.7, but now considering the triangulation surface method.

as in the fourth definition: taking 3 vertexes we can define a plane with a normal vector associated to it. The force applied on each plane is defined as $F_i^{ext} = P \cdot A_i$ where A_i correspond to each area. Subsequently, the force is distributed on the vertexes(atoms) related to the area at same proportions. Equations of motion are obtained by adding this external force to the atomic interactions:

$$m_i \frac{\partial^2 r_{i,\alpha}}{\partial t^2} = F_{i,\alpha} - F_{i,\alpha}^{ext} \qquad \alpha = x, y, z; \quad i = 1, \ldots, N \tag{2.33}$$

where N is the effective number of vertexes (N number of atoms on the surface).
In general, this method could be applied to several kind of structures, hollow or compacted systems, but it doesn't work correctly with structures with big concavities. In our work, we are going to consider structures that don't have these kind of problems.

2.4 Classical pressure reservoir method (Type VI)

In all methods previously mentioned, we have considered an extended Lagrangian adding a term "PV", where volume is evaluated from all atoms or atomic coordinates on the surface. Nevertheless, we also can study pressure effects on finite systems using a more realistic method and corresponds to a variation of a method proposed by *Martonak et al* [14] and originally applied to cluster amorphization ($Si_{35}H_{36}$). In the original implementation, a classical pressure reservoir is put in contact with a cluster (energetically described by first principles). The cluster and the liquid interact classically by fixing the least number of parameters. The liquid serves as a system providing an approximately hydrostatic pressure (if there is a constant density). The equations of motions are derived from classical potentials for the liquid and depending on the cluster description, the potential energy for the cluster is obtained from *ab initio*, tight-binding or even classical potentials (as done in this work). The main constraints in this method are the system size and the maximun pressure limits. The liquid particle numbers has to be large enough to minimize pressure gradients. The interaction potential parameters are not known before the simulation, therefore some testing has to be performed to avoid liquid particles to get into the cluster. The liquid is represented by a pure repulsive potential embedded in a large box with periodic boundary conditions. The Lagrangian representing the coupled system is defined

$$\mathcal{L} = \sum_{i}^{N} \left[\frac{P_i^2}{2M_i} - \phi(R_i) \right] + \sum_{i}^{n} \frac{p_i^2}{2m_i} - \sum_{i,j}^{N,n} V_{I-L}(R_i - X_j) - \sum_{i<j}^{n} V_{L-L}(X_i - X_j) \tag{2.34}$$

where R_i and M_i are coordinates and masses of cluster atoms and X_i and m_i are coordinates and masses of liquid particles. From this Lagrangian, the equations of motions for every particle in the cluster and liquid are obtained.

In order to obtain a hydrostatic pressure, the liquid system particle number must be large enough and also it has to be able to flow quickly to avoid pressure gradients. In the case of pure repulsive potentials, it is well known that for high densities, the liquid could crystallize and the user has to be aware on the choice parameters. They

have to be chosen far as possible from this regime.

The liquid particle potential is a purely repulsive soft-sphere potential $V_{L-L} = \epsilon(\frac{\sigma_{L-L}}{r})^{12}$ where σ_{L-L} is a strength parameter of interaction between two liquid particles. From this potential form, the equation of state has been calculated [23] as

$$p = \frac{N_L k_B T}{\Omega_L}\xi(x) \tag{2.35}$$

where p is the pressure, T is the liquid temperature and the reduced density, x, is given by

$$x = \frac{N_L \sigma_{L-L}^3}{\sqrt{2}\Omega_L}\Big(\frac{\epsilon}{k_B T}\Big)^{1/4} \tag{2.36}$$

It was shown that the liquid system crystallises at $x = x_c \sim 0.8$, where $\xi(x_c) \sim 20$ and it is at a dilute regime at $x \sim 0$ or $\xi \sim 1$ [23]. Note that changing the different system parameters, box size, temperature and particle numbers, the liquid pressure changes. A snapshot of simulation for the case of C_{60} is depicted Fig. 2.9 (Number of particles: 31^3, box size: 36.5^3 angs.).

The cluster-liquid interaction is also represented by a purely repulsive soft-sphere potential $V_{C-L} = \epsilon(\frac{\sigma_{C-L}}{r})^{12}$ where σ_{C-L} is a suitable parameter. This potential has to be large enough in order to prevent possible penetration of liquid particles inside the cluster when high pressures are applied. However this parameter must be suficiently small to avoid a dominant interface tension energy.

Another parameter is the liquid mass, which must exhibit a low value to allow the liquid to adapt to rapid changes and large enough to consider a reasonable time step in our simulations (A more detail presentation of this method and discussion on how to choose the parameters is in Ref. [23]).

In general, parameters are chosen by experience and some previous testing has to be performed before any calculation.

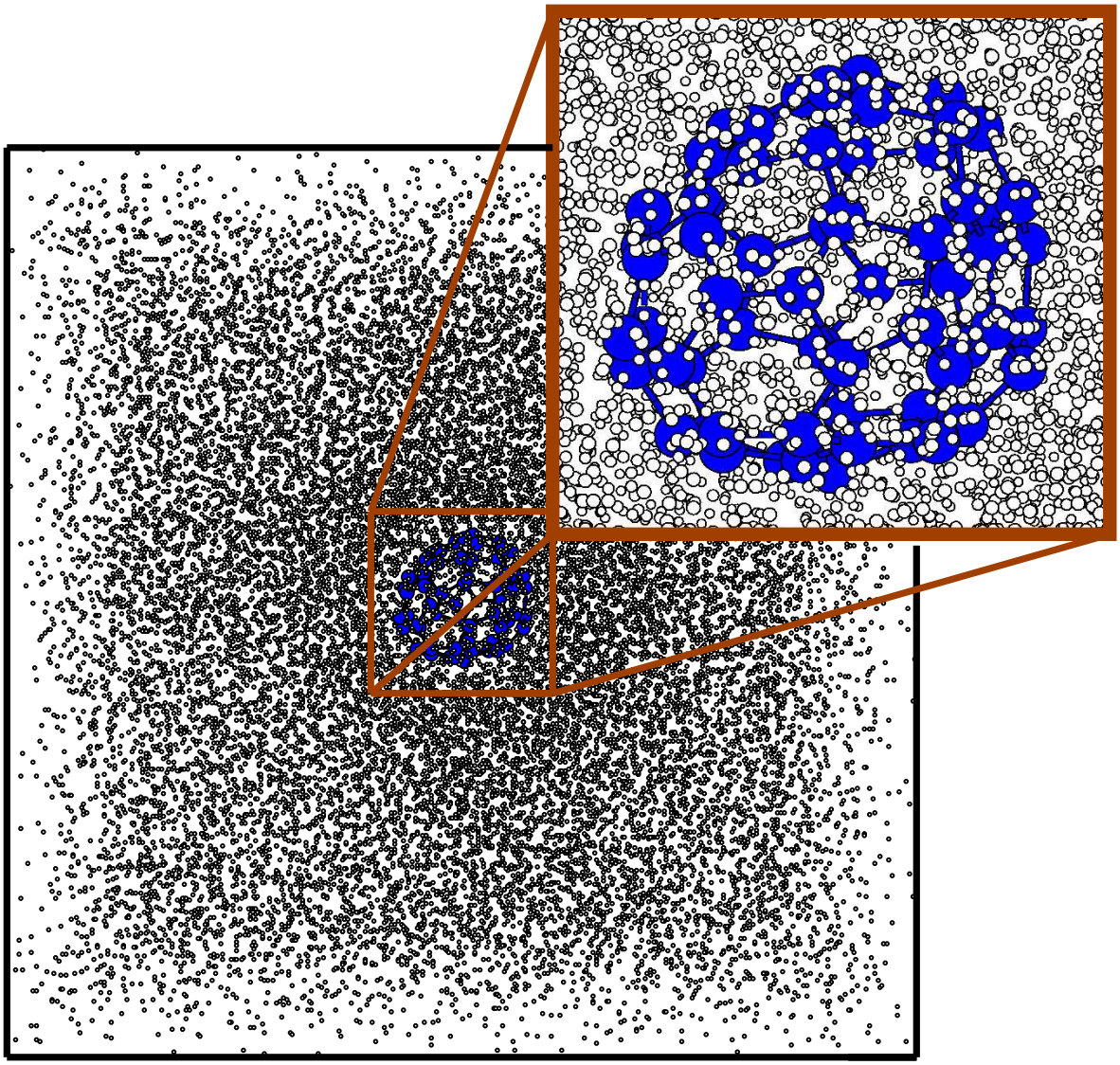

Figure 2.9: Example of Cluster into a liquid system with a detail of the Fullerene C_{60} (Number of particles: 31^3, box size: 36.5^3 angstroms and T: 600 K)

Chapter 3

Implementation

In this chapter we present the algorithms used to model the dynamics under pressure using all diferent approaches introduced in the previous chapter. Our programming language chosen to implement the code has been FORTRAN 90. Different modules were build for every one of these methods and the numerical algorithms for solving the dynamical equations. Simulations were performed in personal computers pentium V with 1 GHz of RAM and a cluster of compute nodes Atipa of 1 Ghz.
We have also divided the implementation of the method in two programs: the first one considers the total coordinates dependence scheme and the volume definitions from surface coordinates. In both cases the structures considered are a non-periodic systems.
A second program was made to include the classical pressure reservoir method which is a periodic system.

3.1 The extended Lagrangian method: total coordinates and surface dependence algorithms

Here we include two approaches to calculate the structure volume; the total coordinates and the surface dependence methods in the same section. This is because both methods consider similar algorithms like the integration method and they have common parameters. Besides, the computational cost associated to the particles number

is lower than the classical pressure reservoir.

3.1.1 Program flux diagram

Fig. 3.1 summarizes the simulation used in the Lagrangian extended method. We have to consider at least two files as program *input files*: the initial coordinates of the system and the parameters selected. These parameters are: external pressure, temperature applied, volume definition considered, simulation time, etc. During the

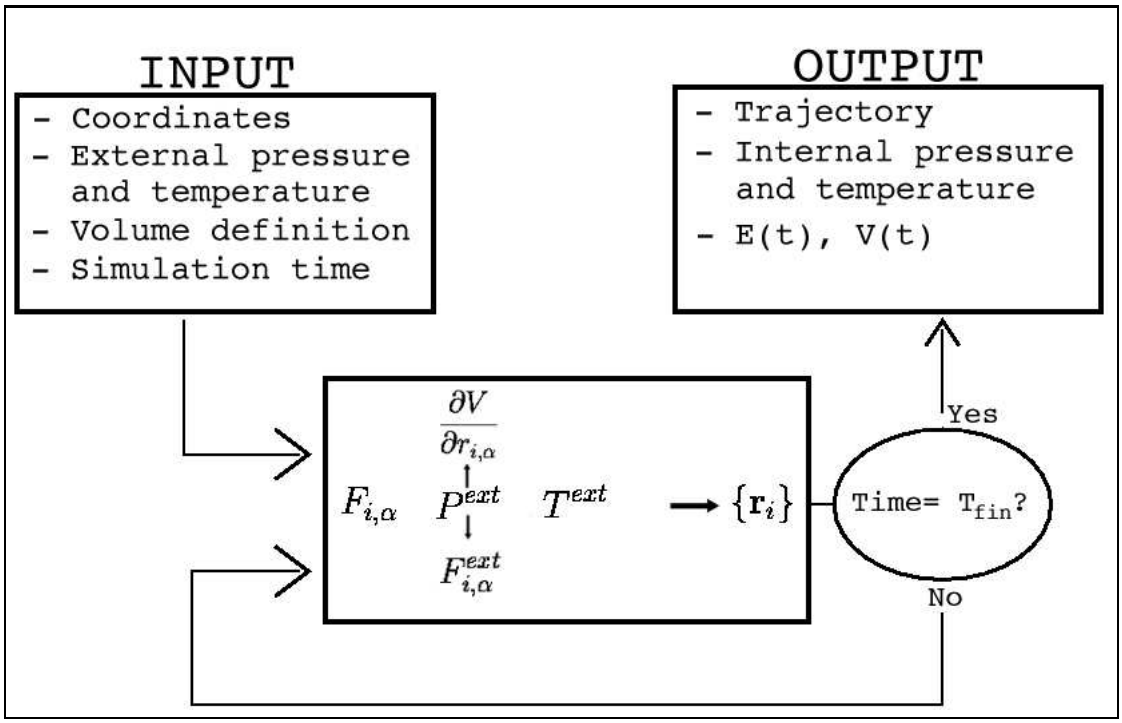

Figure 3.1: The flux diagram of the dynamic simulation. The initial coordinates and the parameters are given to the program as input files.

internal process, our algorithm evaluates the interatomic forces, the process selected to apply the external pressure ($\frac{\partial V}{\partial r_{i,\alpha}}$ or $F^{ext}_{i,\alpha}$), the application of a thermal restriction, etc. The simulation gives the user several *output files*, like for example: trajectory, energy, volume structure, internal pressure and temperature as function of time.

3.2 Classical pressure reservoir method

In this method we have considered periodic boundary conditions. The finite system is embedded in a liquid system that provides the external pressure according to their parameters.

The program requires the cluster initial coordinates and the parameters of the simulation. The parameters considered are cell parameters, temperature of the liquid system and parameter of interaction σ_{LL} between liquid particles. The choice of those, predefined the pressure used into simulation.

The output files are the same as in the previous section: trajectory, energy, volume, temperature, pressure,etc. Every case, the liquid is relaxed until the equilibrium is reached, the inner particles are replaced by the cluster and keeping it fixed until the system is again relaxed.

3.3 The integration algorithm

The integration of equations of motion have been calculated using the method called *Verlet-algorithm* [25, 26]. This algorithm calculates positions and velocities as follows:

$$\vec{v}_i(t+\frac{\Delta t}{2}) = \vec{v}_i(t-\frac{\Delta t}{2}) + \vec{F}_i(t)\frac{\Delta t}{m} \tag{3.1}$$

$$\vec{r}_i(t+\Delta t) = \vec{r}_i(t) + \vec{v}_i(t+\frac{\Delta t}{2})\Delta t \tag{3.2}$$

$$\vec{v}_i(t) = \frac{1}{2}\left[\vec{v}_i(t-\frac{\Delta t}{2}) + \vec{v}_i(t+\frac{\Delta t}{2})\right] \tag{3.3}$$

where the previous velocity is defined by

$$\vec{v}_i(t-\frac{\Delta t}{2}) = \frac{1}{2}\left[\vec{r}_i(t) - \vec{r}_i(t-\Delta t)\right] \tag{3.4}$$

According to the method applied to include the external pressure, the total force on the atom i could be $F_i - P_{ext}\frac{\partial V}{\partial r_i}$ as described in eq. 2.3 if the total coordinates dependence scheme is considered, or it is $F_i - F_i^{ext}$ as in eq. 2.32 if the surface coordinates method is used.

3.3.1 The temperature control

The temperature of the system can be adjusted by using the rescaling velocities method [27]. This method can be added to the Verlet's integration method scaling the velocity $\vec{v}(t - \frac{\Delta t}{2})$ by a factor β as follows:

$$\vec{v}_i(t + \frac{\Delta t}{2}) = \vec{v}_i(t - \frac{\Delta t}{2})\beta + \vec{F}_i(t)\frac{\Delta t}{m} \tag{3.5}$$

where the factor β is equal to

$$\beta^2 = \frac{3(N-1)kT_r\frac{1}{m}}{\sum_{i=1}^{N}\vec{v}_i(t)^2(t - \frac{\Delta t}{2})} \tag{3.6}$$

T_r is the required temperature, N is the number of particles and m is the atomic mass. We have considered a $(N-1)$ factor because the total momenta of the system is zero. This procedure is performed every p iterations and this frequency is diminished each 1000 iterations until rescaling is not necessary to maintain the temperature of the system.

Chapter 4

Results

4.1 Fullerene C_{60} under external pressure

As a prototypical cage molecule and symmetric structure, we have studied the effect of external hydrostatical pressure applied to an individual molecule of C_{60} [28]. This novel structure has been discovered some years ago and it has been widely studied mainly due to its novel physico-chemical properties and possible applications in several areas. An schematic representation of the truncated icosahedral structure of 60 carbon atoms under hydrostatical pressure is shown in Fig. 4.1.

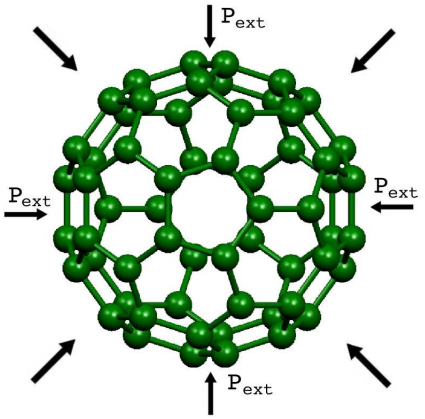

Figure 4.1: The fullerene C_{60} under pressure.

We have applied all different methodologies introduced in the previous chapter (even a non-classical tight-binding simulation) in order to discriminate the performance and the physical meaning of every one fo the discussed methods. In this context, we included as the basic comparison from the algorithm proposed and implemented by *Martonak et al* [14]. They have consider a tight binding energy approximation to the cluster and a classical interaction between the liquid and cluster.

The conditions established for these simulations are:

- For type II (the average interparticle description of cluster volume), we have obtained the initial volume from the initial gyration radii (type III).
- Total simulation time: 100 ps for types I, II and III and a time step of 0.5 fs. Types IV, V, and VII were simulated with a total time of 20 ps with a time step of 0.5 fs. The method VI has been applied considering a total time of 20 ps with a time step of 2 fs. All cases have been relaxed by 5 ps before statistical data collection.
- Definitions I, II, III, IV, V were considered in an isobaric ensemble. In the types VI and VII the dynamic simulations consider an isothermal-isobaric ensemble due to the nature of these models.

The left hand side of Fig. 4.2 shows the normalized average volume change as function of the applied external pressure and after equilibrium has been reached. The right side shows a table of critical pressures associated with each definition. We have defined the *critical or unstable* limit when the fullerene suffers an amorphization so it never returns to a relaxed equilibrium, and the cluster breaks down or collapses due to carbon-carbon bond irreversible breaking. All the curves are depicted in Fig. 4.2 until before the unstable limit, except in cases I and VII where they are beyond the pressure (135 GPa in type I) or the volume ratio (0.88 in Type VII) ranges considered. As seen in this figure, depending on the volume definition, the predicted pressure collapse value for the C_{60} fullerene structure is different. In order to compare the physical behaviour of all different volume definitions, we have considered the trajectory obtained in each simulation and we have taken into account the volume definition of method V (the adapted convex volume definition) to generate the curves reported in Fig.4.2. Methods II, III and IV and VI (tight binding simulation) predict that C_{60} collapses at pressures around 35-40 GPa, compared to the 137 GPa predicted by the first method (type I), 28 GPa predicted using method V and 17 GPa obtained with method VII.

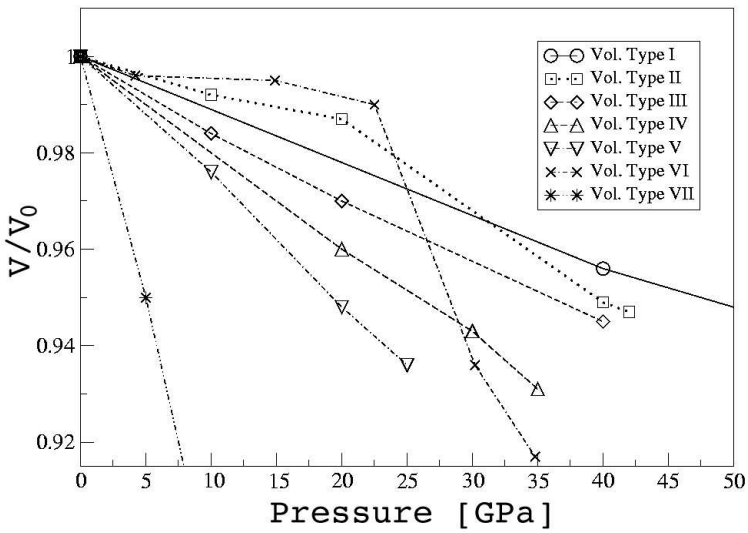

$Vol.def.$	$Pressure$ $[GPa]$
I	137.0
II	43.0
III	41.0
IV	36.0
V	28.0
VI	35.0
VII	17.0

Figure 4.2: Changes of volume as a function of pressure for the different volume definitions considered for a C_{60} molecule. The curves were plotted until the last stable configuration. The right hand side shows the critical pressure of each definition.

The atomic volume definition (type I) shows that the fullerene C_{60} is stable until pressures around 130 GPa. If we compare this behaviour with the reference method (type VI tight-binding) and the rest of the other methods, it is clear the difference in the pressure for diffrent volume definitions. Type II establishes that C_{60} is stable up to 42 GPa, whereas the third case, Type III, reveals that the system maintains its stability at pressures lower than 40 GPa. The Volume defined from the surface coordinates (type IV) is stable until reaching 35 GPa. The adapted convex volume definition (type V) has a limit close to 25 GPa. The classical pressure reservoir approach (type VII) is stable until 15 GPa of external pressures.

Methods II, III, IV, exhibit critical pressures similar to the predicted pressures using tigth-binding calculations. tight-binding method. The method V indicates a lower critical pressure than the reference method, but this could be for a different reason. The reference method has considered an external pressure given by a classical reservoir, in which the pressure on the whole structure is equal, in average, to the external pressure, where as for the adapted convex volume definition, each face (defined by three vertexes) distributes the force applied on its surface to each vertex atom. In this context, it is feasible to expect a critical pressure less than

in the reference case due to the fact that the supported pressure in every face is exactly equal to the applied pressure. In definition VII (classical approach of the pressure reservoir), we have found that the particle number in the liquid system is critical in order to avoid gradient pressure effects. This could be the main problem of this approach and the reason to obtain a smaller value of a critical pressure and a smaller critical volume ratio. In the case of type IV, we obtain a pressure that is close to the methods II, III as well as the reference method (Even though, there is a potential problem). The faces are defined by the minimal number of vertexes used in the convex volume definition excluding coplanar points and points that belong to the concave surface, and we think, this effect can change details of the dynamics.
In addition, the reference method, obtained using a tight binding calculation to described which is embedded in a pressure reservoir, has to include a large number of liquid particles so the simulation time increases by a large factor respect other methods.

In order to verify the equilibrium relaxation, we have followed the volume changes and internal pressure as function of time for type III as shown in Fig.4.3. It is clear, that volume and pressures oscillate around the equilibrium value as function of time. The dynamical behaviour reveals several vibrational excitations on the fullerene, with decreasing radial amplitude as function of pressure. This is a clear indication, that forces in the radial direction are responsible of maintaining the cluster in equilibrium until the pressure is larger than the extended forces that are not able to keep the fullerene structure.
It is clear from our analysis, that type I and type II predict in agreement the dynamical behaviour of caged structures under pressure but they overestimate the critical pressure required to break the structure.
From now on, we will not include these definitions (except type II in next section) in our subsequent calculations. When a finite system is submitted to a large hydrostatic pressure, "anisotropies" can be part of the dynamics and a method which contains those features is more relevant. In the case of type IV, as long as the structure does not show concave behavior, the method is well adapted; but as we shown in other examples, concave geometries are quite frequent and this method

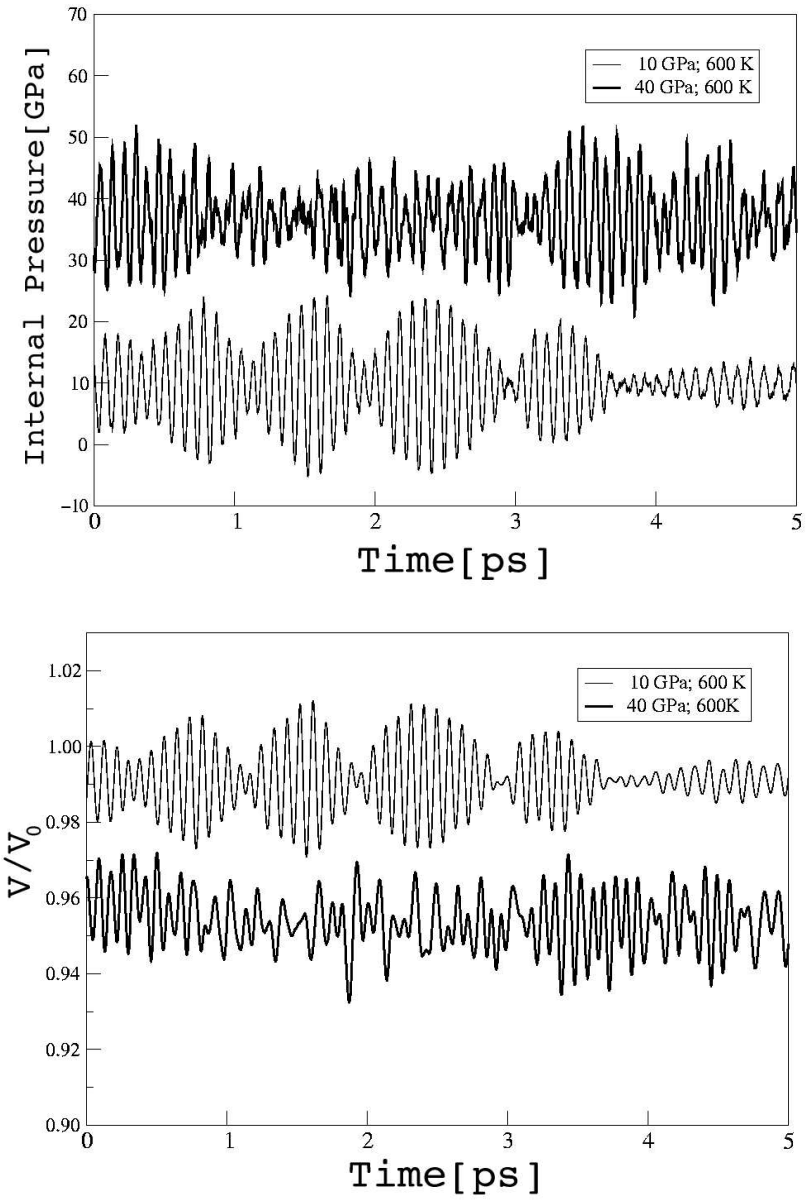

Figure 4.3: Pressure and volume as functions of time for C_{60} at 600 K. The applied external pressures are 10 GPa and 40 GPa as shown in the insets

could lead to wrong conclusions.

4.2 SWCNT under external pressure

In this section, we have considered the effects of an external pressure on single salled carbon nanotubes (SWCNTs). These novel structures identified by Iijima [38] have been widely studied due to their fascinating properties and applications in several fields. These structures are produced by several methods like: Carbon arc discharge [39], pulsed-lased vaporisation [40], chemical vapour deposition [41, 42], etc. The theoretical stability and electronic properties of these structures have been reported but in several papers [32, 33], but mos of the studies have been performed in a periodic frame. In this situation, the tube is considered as an infinite open tube along the tube axis, i.e. without caps.

Pressure effects on SWCNTs have been also studied considering a periodic framework [35, 36]. A measurement of the SWCNT compressibility in a hexagonal closed packing lattice of 1.4 nm diameter tubes has been reported by Tang et al [34] and found a stability upper limit of 4 GPa to an external pressure.

The properties derived from periodic models could be different from the finite case. In this work, we consider a caped carbon nanotube armchair (5,5) (as the ones shown in Fig. 4.5), The cap is obtained by introducing carbon pentagons and hexagons in a spherical shape (half C_{60}). The (5,5) nanotube has been used to demostrate different effects of two volume definitions: the average description of cluster volume (type II) and the volume from gyration radii(type III).

As discussed previously in chapter 2, these definitions affect the equations of motion in a different form. One of our goals it is to show the mechanical deformation of a SWCNT as function of pressure. In the case of a nanotube, this deformation is larger than in C_{60} fullerene and happens in both axial and radial directions. In Fig. 4.5, we have considered an armchair nanotube with 370 atoms. It has a diameter of 7.1 Angs. and a length of 45 Angs.

The conditions of these simulations were:

- Total simulation time: 15 ps. First 5 ps. for relaxation, 10 ps of statistical data collection. The time step is 0.5 fs.

- The simulation was developed considering an isobaric ensemble (no temperature restriction).

- Whereas the dynamic behaviour is controlled according to each volume definition (the term $\frac{\partial V}{\partial r_i}$), the calculated volumes have the same definition in both cases: the volume from gyration radii.

- The Initial volume V_i given as parameter in definition II and calculated according to definition III.

The Figure 4.4 shows a comparison of the deformations experienced by the nanotubes as function of pressure for the two volume definitions (type II and type III). The volume change (a) and the total energy (b) are shown as functions of the hydrostatic pressure until a critical pressure, in which the nanotube collapses. The top graph indicates that depending on the volume definition, the deformation results in a different value, which is not the case for C_{60}, where no anisotropy is present. In the case of the average distance volume (type II), the critical pressure is much lower than the case of the gyration radii volume. This is mainly due to the fact that in the former case, the volume is mapped on a spherical shape and there is no record on the volume itself to have that symmetry.

The energy per atom, on the right hand side of this graph, confirms the different effects of each simulation. Initially, the two volumes show similar behaviour (almost a linear change of total energy as function of pressure) but the system starts to experience different behaviour as the pressure increases. Thus the nanotube starts feeling different dynamics with respect to the main axial direction. Phonons along the tube axis are excited more efficiently if the volume definition accounts for the asymmetry. These phonons are able to aid the tube stabilisation and the critical pressure occurs at a higher value. We conclude that the volume definition type II is unable to reproduce physical behaviour in anisotropic structures for extreme pressures.

From Fig. 4.4, one could observe the nonlinear volume dependence of the pressure, which is an important feature of systems that are not in thier elastic regime. The deformation occurs in the axial direction, where there is a compression and on the

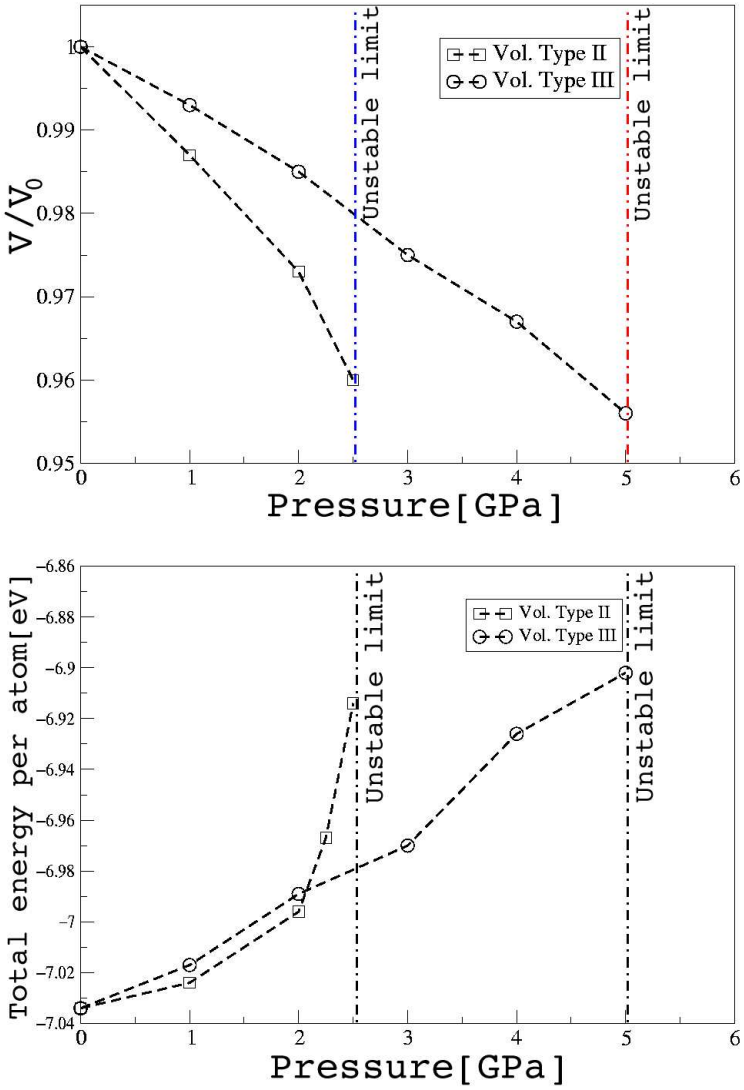

Figure 4.4: (a) Volume as a function of pressure for a caped (5,5) nanotube.(b) Total energy per atom for a caped (5,5) after a relaxation of 5 ps. The curves were drawn until experiencing unstable configurations.

nanotube center where there is a transition to a peanut shape. The caps does not show any deformation (remember that C_{60} collapses at around 35 GPa). Finally, a summary of the structural changes caused by an external hydrostatic pressure applied to a (5,5) nanotube are presented in Fig.4.5. The dynamical simulations corresponds to the isobaric ensemble that uses definition III.

This figure (4.5), starts with the initial nanotube enclosed by caps obtained with hexagons and pentagons. When the hydrostatic pressure increases, the middle of the

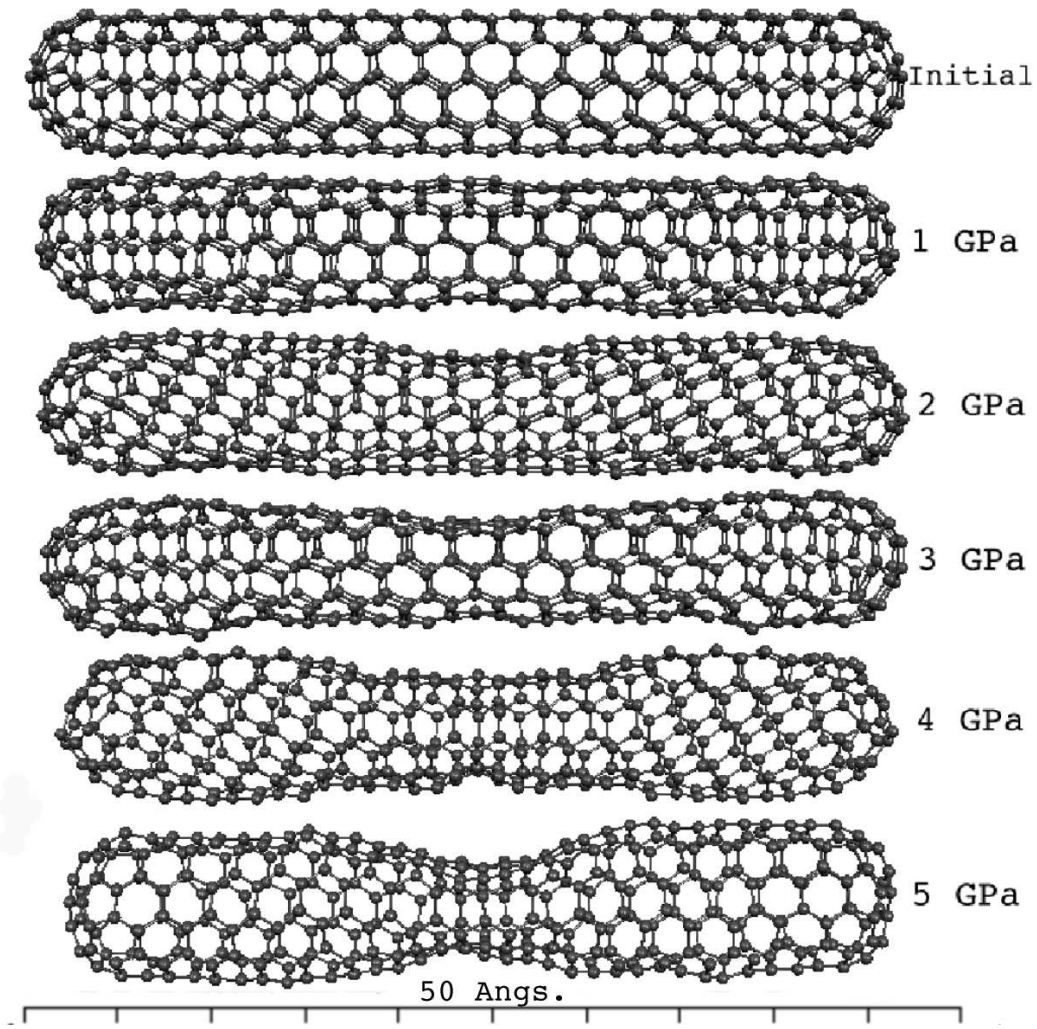

Figure 4.5: SWCNT at different external pressures.

nanotube starts to be compressed, affecting of the radial pressure and the pressure exerted at the caps. This effect can be attributed to the anisotropy of the tube which provides a rigidity along the tube. This fact can be clearly observed when the pressure increases until a critical value of collapsing.

Another interesting simulation approach would be to consider the definition of volume according to the adapted convex volume, because it could maintain a pressure on each face defined on the surface that can be convex or concave. This calculation is not included in this work.

4.3 Nanodiamonds under external pressure

A type of compact carbon structures is a diamond-like cluster also called *nanodiamond*. They can be found in different symmetries and they can have different reactivities depending on how their surfaces reconstruct. In order to use this type of system various volume definitions should be tested. We have started considering a spherical nanodiamond, which is built by taking a crystalline carbon diamond system and resahping it into a spherical cluster by a given radius. The geometry is optimized by using tight-binding methods, in order to relax the structural surface. After a nanodiamond has been obtained, we use this as input file in our simulation. The dynamical simulation has been performed by using the volume definition III (or volume generated from the gyration radii). This was chosen due to the results obtained from our previous analysis of C_{60} and single walled carbon nanotube simulations.

The conditions applied to these simulations were:

- The dynamical simulations correspond to an isothermal-isobaric ensemble.
- The simulation time is 15 ps: 5 ps. of relaxation and 10 ps to collect the statistical data.
- The temperature of the system is scaled with a velocity Verlet algorithm every 30 iterations.

Using the volume definition called gyration radii definition (Type III), we have studied finite carbons systems. To perform this study we have considered two nanocrystals of carbon diamond; the first one considers a system of 441 atoms and the second is the same system but without a central atom (440 atoms).

4.3.1 Nanodiamond A

The conditions applied to this nanocluster are: external pressure of 50, 100, 200 GPa and temperature of 300 K, 600 K and 900 K.

Our first observation is basically that the nanodiamond suffers a transition from the

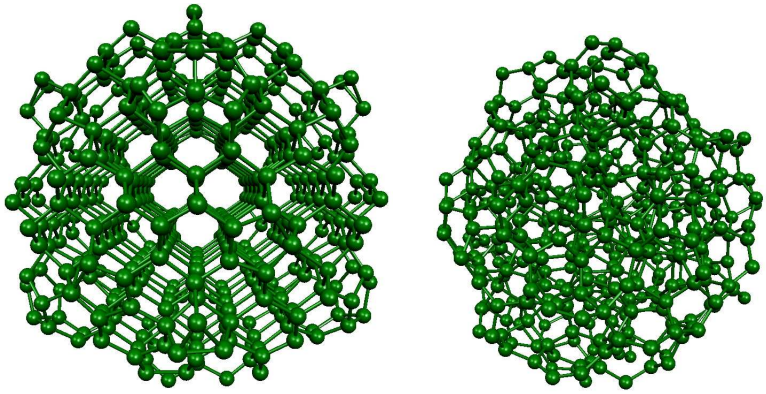

(a) (b)

Figure 4.6: (a) Model of a nanodiamond with 441 atoms.(b) Amorphous phase at temperature simulations of 300 K, and 10 ps of data were collected after 5 ps of relaxation.

ordered structure (sp^3 hybridisation in volume) to a more disordered phase, with sp and sp^2 present. This transition occurs at 100 GPa. The predictions on the transition depend on the method used. For example the method of atomic volumes (type I) predicts a transition structure at pressures higher than 200 GPas whereas method II and III show a different critical pressure. We should conclude that the most accurate volume definition we have used predicts transition at a pressure close to 100 GPa. Figure 4.6 shows the initial and the final configuration of the nanodiamond after applying a pressure of 100 GPa.

In order to characterise the quality of the amorphous carbon structure obtained from our simulation, we have performed an analysis of the average coordination number as function of pressure and temperature (see table 4.1). The second column corresponds to the initial percentage of coordination numbers. We notice that there is an important variation when the external pressure changes from 50 to 100 GPa (at 300 K). It is noteworthy, that the temperature helps to obtain rather uniform amorphous carbon, The number of carbon with coordination number 4 has decreased from 58.7 % to 20.2 % at 50 GPa-300K and 100 GPa-300K respectively (see table 4.1). The number of carbon atoms with coordination 3 has been enhanced, showing the strong amorphization happening in the sample. There is no major change between 600 K and 900 K, indicating that the system is stable. This has important implications

on the manufacture of disordered systems (which are very interesting due to its electronic properties and applications to integrate biological systems with electronic devices [60]).

Table 4.1: Percentage of coordination number in Nanodiamond A

N	Initial	**300 K**			**600 K**			**900 K**		
		Pressure [GPa]								
		50	100	200	50	100	200	50	100	200
0	0.0	0.0	0.0	0.0	0.0	0.0	0.0	0.0	0.0	0.0
1	0.0	0.4	0.2	0.0	0.4	0.2	0.2	0.4	0.2	0.2
2	5.4	7.3	10.7	11.6	14.1	15.2	12.5	21.9	15.2	12.5
3	37.2	33.6	48.3	48.5	65.3	58.7	51.9	69.9	58.7	51.9
4	57.4	**58.7**	40.8	39.9	**20.2**	25.9	35.4	7.8	25.9	35.4
5	0.0	0.0	0.0	0.0	0.0	0.0	0.0	0.0	0.0	0.0

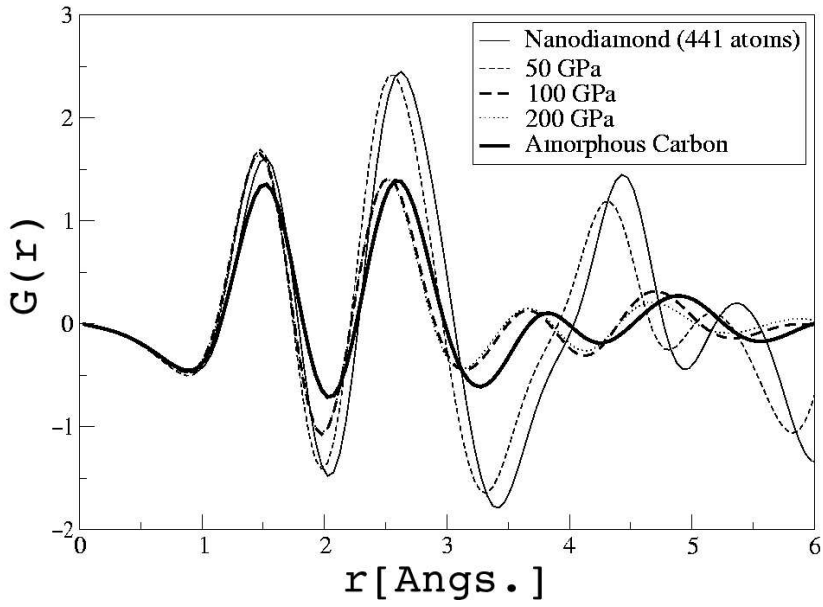

Figure 4.7: Reduced Radial Distribution Function of nanodiamond A (441 atoms) under external pressure at 300 K.

In order to describe the transition of nanodiamond to an amorphous phase, we have calculated the reduced radial distribution function (RDF) of the system before and

after the pressure is applied and compare it with the RDF of a model of amorphous carbon [61] (a discussion on how RDF is calculated is presented in appendix I).
It can be seen from Fig 4.7 that between 50 GPa and 100 GPa there is a transition from the diamond phase to an *amorphous* one. The radial distribution function of our amorphous nanodiamond is in good agreement with the amorphous phase until the 4^{th} peak position. After that distance, the surface effects of our finite system starts to appear, thus contributing to different peaks.

4.3.2 Nanodiamond B

In this case we have considered the effects of external pressure applied on a nanodiamond without the central atom (440 atoms). We have also calculated the percentage of coordination number which is shown in table 4.2.

We have performed dynamical simulations considering pressures of 100 GPa, 200 GPa and 300 GPa and temperatures of 300 K, 600 K and 900 K. As we can see, in

Table 4.2: Percentage of coordination number in Nanodiamond B

N	Initial	**300 K**			**600 K**			**900 K**		
		Pressure [GPa]								
		100	200	300	100	200	300	100	200	300
0	0.0	0.0	0.0	0.0	0.0	0.0	0.0	0.0	0.0	0.0
1	0.0	0.0	0.0	0.6	0.2	0.0	0.2	1.0	0.8	1.4
2	5.5	11.8	10.9	11.6	14.5	15.1	13.1	20.0	18.7	15.8
3	38.2	51.4	50.9	51.0	62.5	52.6	49.6	67.1	64.9	60.1
4	56.3	36.8	38.2	36.8	22.7	32.3	36.5	11.8	14.9	21.5
5	0.0	0.0	0.0	0.4	0.0	0.0	0.6	0.1	0.7	1.2

this situation, hydrostatical pressure effects have been observed and they produces a change of the percentage of coordination number 3 and a diminishing of coordination number 4 respect to the initial conditions (second column).

The temperature also favours an amorphization of nanodiamonds, thus altering the changes of the carbon coordination numbers. The lack of a central atom reveals a diminishing of the coordination number 4 respect to the nanodiamond A case (see previous section), indicating that vacancies could help amophization. This result could be attributed to an energetically instability produced by the vacancy located in the centre of the structure.

4.4 Onion-like carbon structures under external pressure

In this section we have have considered a concentric fullerene system also called a *nano-onion*. This cluster can be obtained by putting together several fullerens such that the distance between two consecutives ones is of the order of 3.4 Å.

The Figure 4.8 shows an example of these structures considering only 3 layers: the inner layer is C_{60}, the intermediate graphitic layer is a fullerene of 240 carbon atoms with a diameter of 14 angs. and an external layer containing 500 atoms ($C_{60}@C_{240}@C_{500}$). All these structures possess icosahedral symmetry

The structural transformation of graphitic onions into diamond nanoclusters have been previously reported by *Banhart and Ajayan* [43, 44]. These nanocrystals were obtained under electron irradiation from concentric carbon shells of many layers.

We have considered an onion structure of 800 carbon atoms (3 layers) and applied an external hydrostatic pressure using the volume definition obtained with the gyration radii (type III).

The systems has been considered in a dynamic simulation under pressure at different

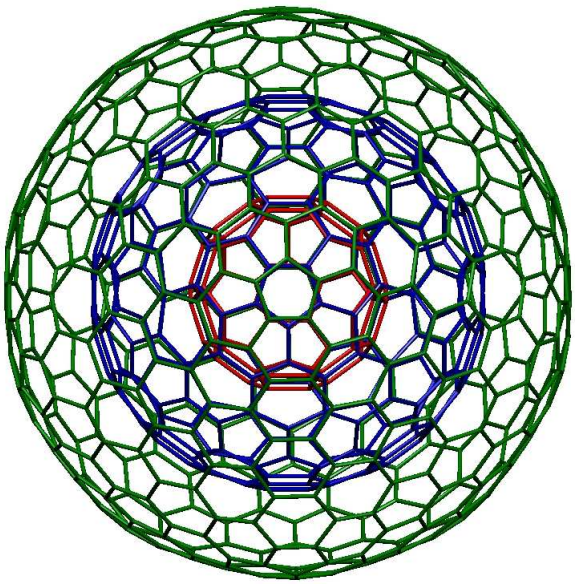

Figure 4.8: Example of a concentric fullerene structure of 3 layers (these layers are drawn with different colours).

temperatures (300 K and 600 K).

Figure 4.9 shows the change of the percentage of coordination numbers in concentric fullerenes and a final configuration of the nano-onion when 50 GPa of external pressure is applied at 300 K. The second column of the table corresponds to the initial coordination numbers where the graphitic structure is clear (all atoms with coordination number 3). When the pressure is applied, a transition of the coordination number occurs. These effects are enhanced when the temperature is higher and these changes favour an increase of the coordination numbers 2 and 4.

These results demostrate that the effect in this structure, due an external pressure,

N	Initial	**300 K**		**600 K**	
		Pressure [GPa]			
		50	100	50	100
1	0.0	0.9	0.9	1.2	1.4
2	0.0	12.4	12.6	17.3	15.1
3	100.0	64.4	47.5	61.7	50.8
4	0.0	20.9	33.6	17.0	26.4
5	0.0	1.3	4.0	2.2	4.9
6	0.0	0.1	1.3	0.4	1.4

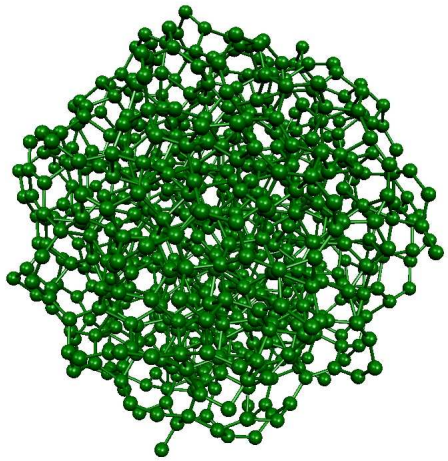

Figure 4.9: Coordination number percentage in concentric fullerenes and a snapshot of the final structure of $C_{60}@C_{240}@C_{500}$ at 50 GPa and 300 K.

is the amorphization of the carbon structure. The situation occurs at both temperature (300 K and 600 K). These transitions can be seen when the reduced radial distribution function is calculated (see fig. 4.10). This figure shows the pressure effects at 50 GPa and 100 GPa. The amorphization of the structure is obtained when the nano-onion is under an external pressure and obtained structures look very similar at 300 K and 600 K. It is also clear that the nanodiamond considered (441 atoms) has a RDF very different to these results, therefore, it is not possible to detect the formation of diamond-like cluster using the definition type III.

One problem in our calculations, is the fact that only 3 graphitic layers were considered and C_{60} (the inner layer) is rather reluctant to break; a larger number of shells

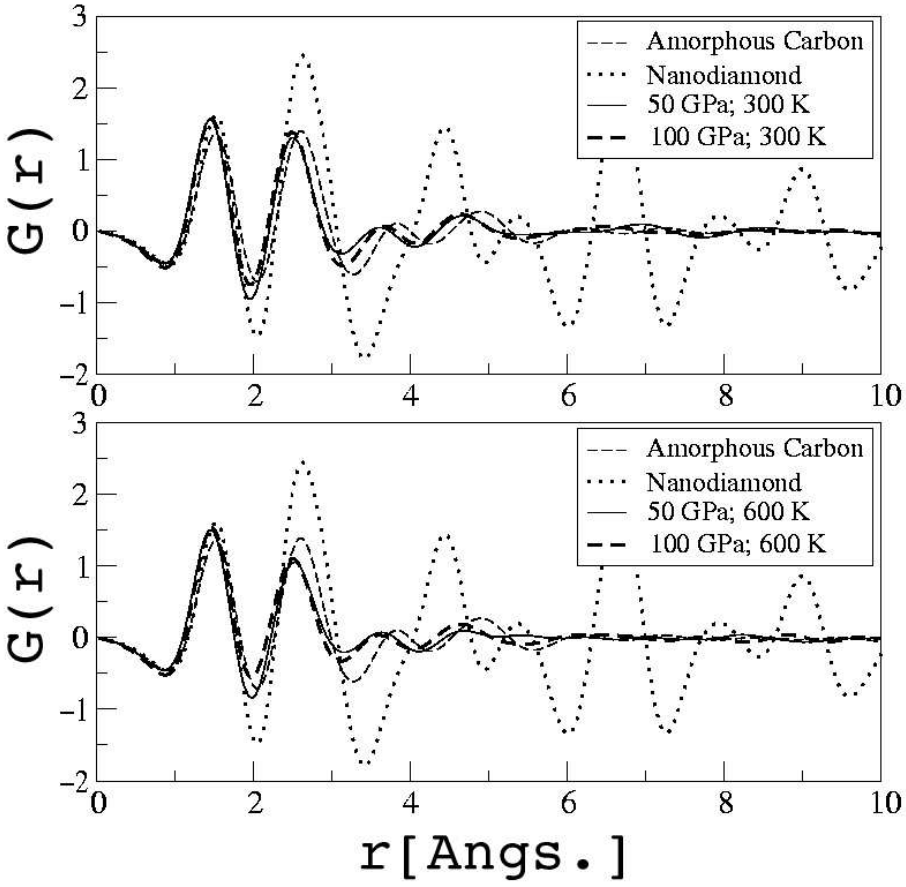

Figure 4.10: Radial Distribution of Onion Structure (800 atoms) under pressure and temperature. Also it is compared with a nanodiamond of 441 atoms and a amorphous carbon phase

should be used to make more general statements. Experiments have demostrated that such onions contains several shells (more than 10).

4.5 Gold Clusters

4.5.1 Symmetries

In this section we study the effects of pressure on finite metallic systems. In particular we are interested in the structural transformations of mono-metallic clusters under pressure.

These effects have important implications, because they could help to design nano-sized objects with novel applications due to its surface properties or to stabilise systems that are metastable under normal conditions. Finite systems such as metallic clusters have interesting feature, for example, these structures exhibit symmetries (icosahedral—I_h or decahedral—D_h) that are prohibited in standard crystallographic systems where translational symmetry is essential (a brief introduction about finite symmetries is in appendix 2).

Structural transitions in clusters have been experimentally reported by Iijima *et al.* [37]. These transformations were induced by irradiation of an electron beam on gold particles, obtaining a transformation from single crystal to a twinned crystal and viceversa. Since then, it is well stablished now [46], that structure fluctuations are nevertheless thermally activated, due to its internal cluster temperature, which is one of the most elusive experimental parameters. Temperature effects on gold particles have been experimental and theoretically studied [47, 51].

Some of these transitions could also be understood within the context of an applied external pressure. The study of silver clusters under pressure has been recently reported by Calvo and Doye [13]. In this case, they used an approach to the volume system that depends of the convex volume [30] and they have found that structures with fcc symmetry (O_h) are more stable than structures with icosahedral (I_h) or decahedral (D_h) symmetries. The geometric characteristics of the clusters formed by concentric layers can be considered, as formed by equivalent sites: sites located at the same distance from the origin, which occupy the same geometric place and have the same environment (the same number and type of neighbours). These layers can be arranged in such a way that they group in shells forming clusters of different sizes, retaining the original geometric structure. The number of shells in the cluster

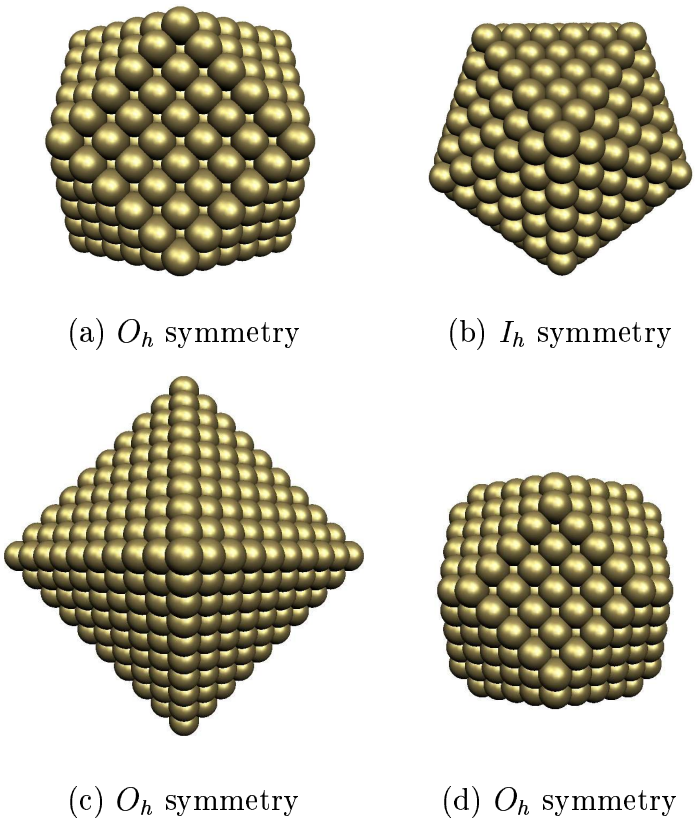

(a) O_h symmetry (b) I_h symmetry

(c) O_h symmetry (d) O_h symmetry

Figure 4.11: The optimized structures and symmetry (Schoenflies notation) of gold clusters studied in this work: (a) icosahedron and (b) cuboctahedron clusters both with 561 atoms, (c) truncated octahedron with 490 atoms, and (d) octahedron with 670 atoms.

is called the order of the cluster. Now we know that clusters are atomic structures formed by shells, and the concept of a magic number can be introduced [54, 55]. Several gold clusters are shown in Fig. 4.11. They correspond to the the icosahedron (b) cluster that belongs to the icosahedral group; the most symmetrical point group (see appendix B), whereas the cube-octahedron (a), the octahedron (c), and the truncated octahedron (d) belong to the octahedral symmetry group. The symmetries of all of our final metallic structures under pressure studied here were verified by means of a computational package [31], in order to determine accurately (and not just visually) structural transitions. Alternatively, we have calculated the reduced radial distribution function (RDF) curves with the same purpose (see Appendix A). Figure 4.12 shows the $G(r)$ functions for each considered cluster. The main information we obtain from these curves is the average atomic distance (first, second

and so on nearest neighbours). Therefore, changes or displacements of the main peaks in the curves reflect different structural environments. In this case, due to the fact that the octahedron, the cuboctahedron and the truncated octahedron have all the same symmetry (O_h; fcc packing), , and because the clusters are not still under pressure, we observe two kind of curves, one corresponding to this fcc atomic packing and another corresponding to a cluster with I_h symmetry. In this figure, note that, the significative differences start at the second and third nearest neighbors peaks (between 5 and 6.5 Å). We will use these $G(r)$ curves as references to detect structural transformations under pressure. First, we are going to discuss the results for the icosahedron, the cuboctahedron, the truncated cuboctahedron, and finally, the octahedron. As we mentioned before, besides a visual exploration of the final structure, we performed an analysis of the structure by means of the $G(r)$ functions. Simulations were performed within the isobaric-isothermal ensemble (NPT) with a time step $\tau = 5$ fs and a total simulation time of 100 ps. All the simulations were performed at 300 K, though a more systematic study is necessary and simulations in this direction are underway for these systems. Although in the situations of nonperiodic compact systems, like the metallic clusters in this section, the volume definition is not crucial (as in hollow systems). The volume definition we have applied throughout all the simulations in this section, was definition III or volume obtained from gyration radii.

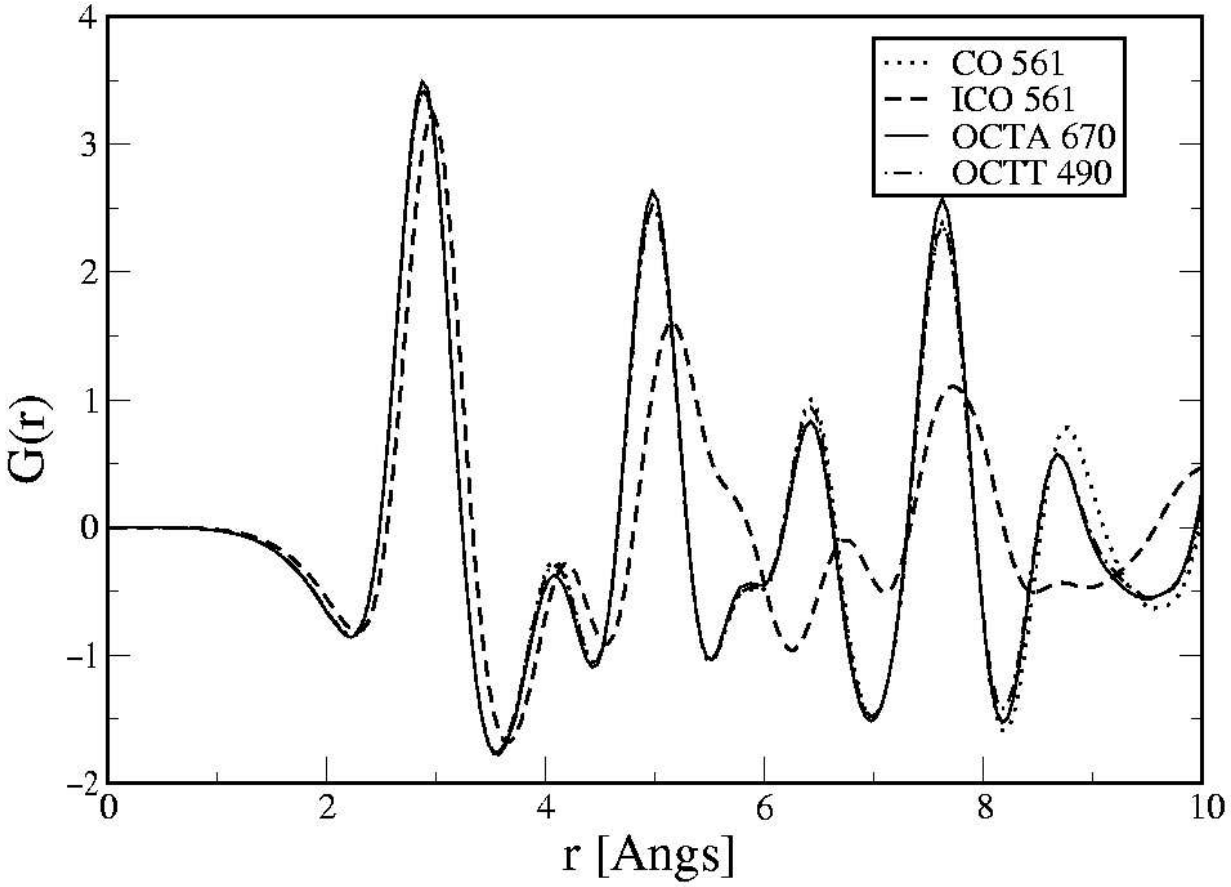

Figure 4.12: Summary of reduced radial distribution function ($G(r)$) of different gold clusters studied at pressure $P = 0$. We have basically two curves corresponding to icosahedral and octahedral (fcc) symmetries.

4.5.2 Icosahedral cluster

We have applied different pressure values to this cluster ranging from 0 GPa up to 80 GPa, at temperature of 300 K and have not found any significant structural transformations in this pressure range.

This result is expected in some way because clusters with icosahedral symmetry are the most energetically stable at this size range [51], and Figure 4.13 shows the $G(r)$ function for this structure under an applied pressure value of 80 GPa, and the only significant feature is the compactation of the cluster due to this high pressure.

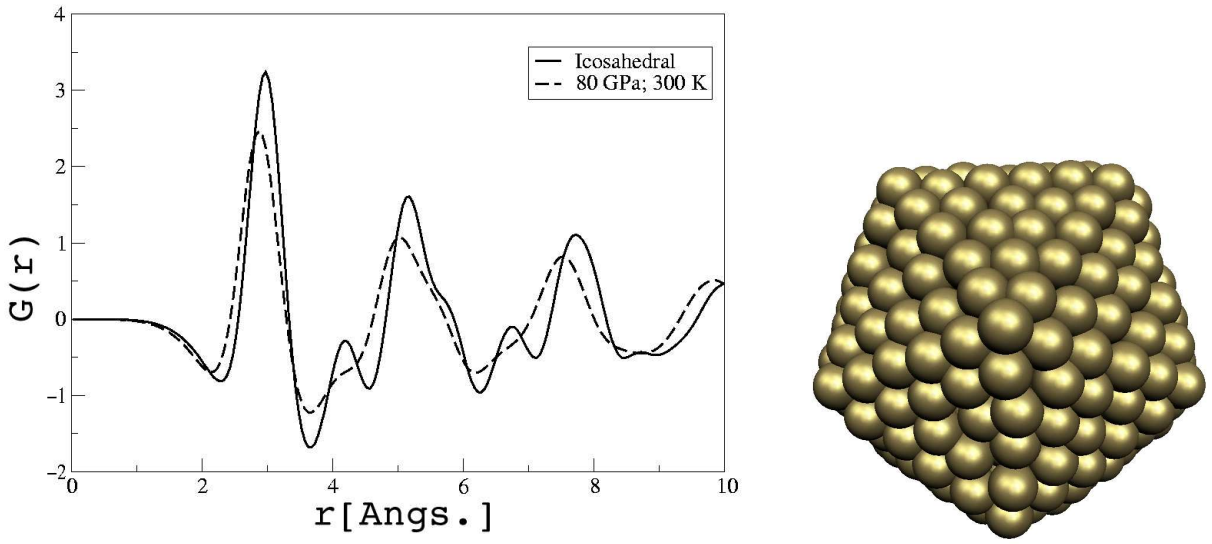

(a) (b)

Figure 4.13: (a)Radial Distribution Function of Icosahedral cluster under 80 GPa at 300K (561 atoms). Also we added the RDF of Initial configuration.(b) A snapshot of the final configuration.

The main peaks that characterise the icosahedron cluster in the reduced RDF curve still remain.

4.5.3 Cube octahedral cluster

The O_h symmetry is the most competitive energetic atomic packing compared to the I_h atomic packing [55]. Both experimental [37] and theoretical [13] studies have shown that these atomic arrangements compete between them in this small nanometer range. However, for metallic nanoparticles, decahedral and icosahedral structures are favoured in the very small size range (1-5 nm), after that the most stable structure exhibits fcc symmetry, unfortunately this structural size frontier has not been yet precisely determined. Structural transformations from the cuboctahedron to the icosahedron have been reported before by means of a myriad of theoretical studies [50] and simulation methods like classical molecular simulations [45] and experimental techniques [48,49]. In Fig. 4.14 we present structural transitions from the cuboctahedral to the icosahedral cluster induced by pressure. We show two

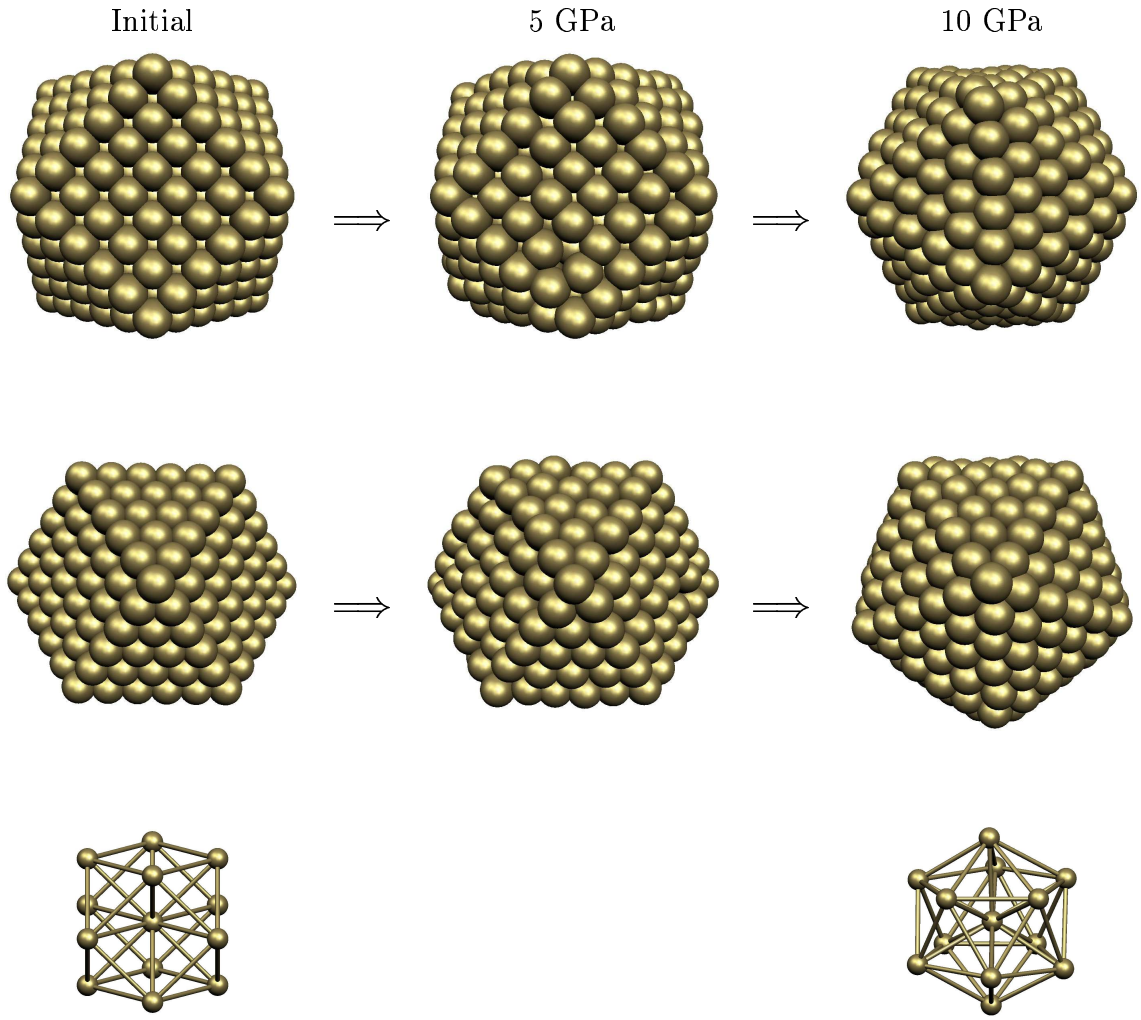

Figure 4.14: Two different symmetry axis viewpoints showing the initial cuboctahedral clusters of Au (561 atoms) and at subsequent applied pressures of 5 GPa and 10 GPa at a temperature of 300 K. Note how the structural transition is induced between these range of pressures. Third row shows their core structures (13 atoms) that evidences the deep structural transition.

different symmetry axis snapshots of the cuboctahedral cluster showing the initial configuration and the same for subsequent applied pressures of 5 GPa and 10 GPa at a temperature of 300 K. Notice how the structural transition is induced between these pressure ranges. We illustrate in the third row their core structures that evidences this structural transition. Figure 4.15 shows the RDF curves that indicate the effect of pressure within the structure. There is no doubt about the structural transformation from cuboctahedral to icosahedal symmetry. The small shifts on the

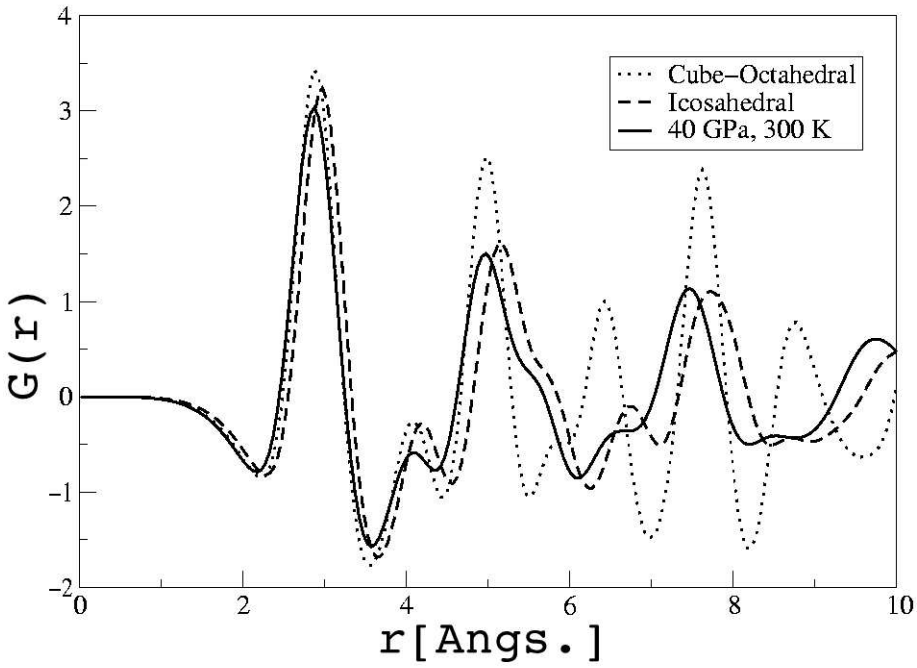

Figure 4.15: Radial distribution function of cuboctahedron under 40 GPa at 300K (561 atoms). For comparison, we added the RDF of the initial configuration and the icosahedral cluster with 561 atoms. It is evident the structural transformation under pressure.

main peaks of the curves are consequences of the applied pressure which compacts the structure. This transition is stable when the external pressure is removed.

4.5.4 Truncated cuboctahedron cluster

We have performed simulations in this cluster (490 atoms) with different parameters (like increasing the system temperature, increasing the pressure (0-80 GPa) and slowly liberating the pressure down to return to 0 GPa) in order to explore if transformations are induced changing these conditions.

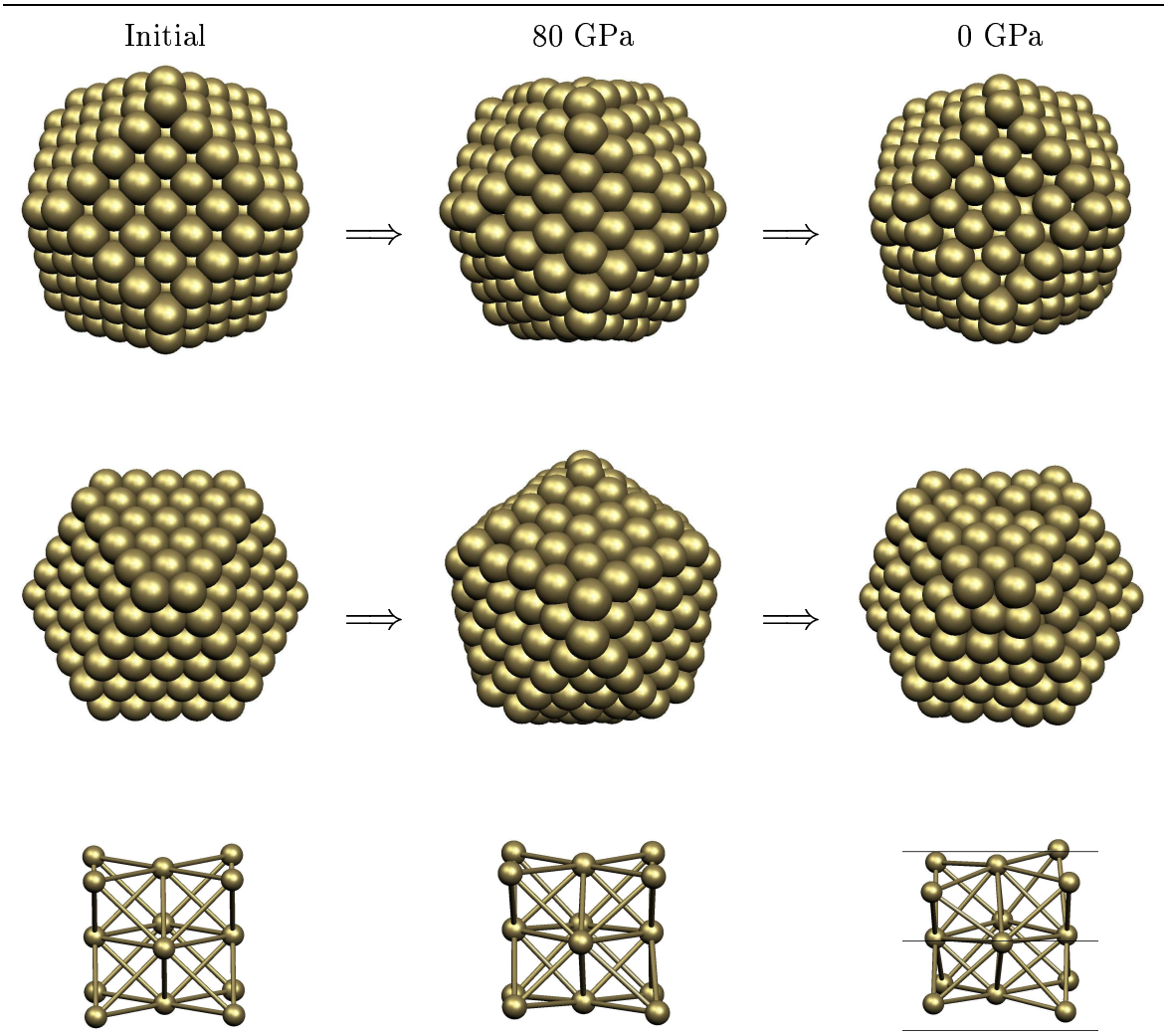

Figure 4.16: Two different axial symmetry snapshots for the truncated cuboctahedral cluster with 490 atoms at 300 K of temperature, as well as their core structures (14 atoms). In this case, no significant structural changes are observed in the wide range of pressures applied.

The result of apply this simulation is presented in Fig.4.16. Although there are not strictly structural changes on the cluster under pressure, visual exploration of the final clusters shows some interesting features. For example, there is a surface reconstruction on the cluster that resembles a cluster with icosahedral symmetry, but the core of the particles still has the octahedral symmetry. Also, after relaxation of the whole structure, it remains distorted and returns to the original configuration. The analysis of the RDF (see Fig. 4.17)reflects only the usual shifts peaks because of pressure effects, but not strictly structural changes in this cluster.

This transition is not stable when the external pressure is removed, and it returns to a configuration that is similar to the truncated octahedral.

A more systematic study in this direction is underway.

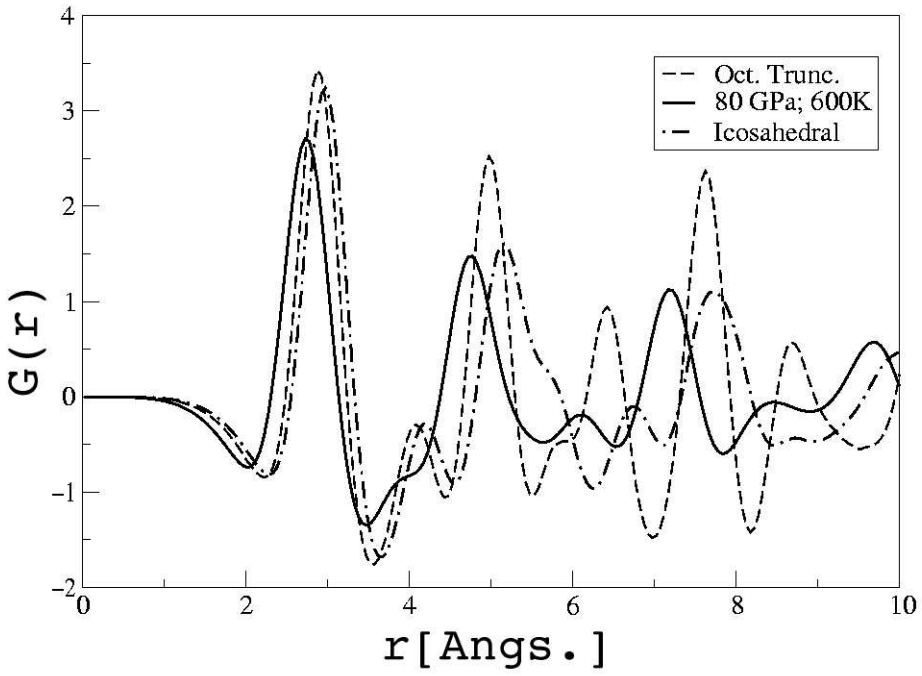

Figure 4.17: RDF of Octahedral truncated under 80 GPa at 600K (490 atoms). Also we added the RDF of Initial configuration and the RDF of Icosahedral cluster (561 atoms).

4.5.5 The octahedron cluster

The last system is the octahedron cluster (670 atoms) and it doesn't present a significant structural change when the external pressure is applied.

Regarding the regular octahedron, after a wide range of pressures (from 0 to 80 GPa) is applied, and at 300 K, the structure also remains with the same symmetry. The reduced RDF and the final configuration are shwon in Fig. 4.18. We notice some migration of surface atoms took place, creating surface vacancies and islands and steps in other places on the surface.

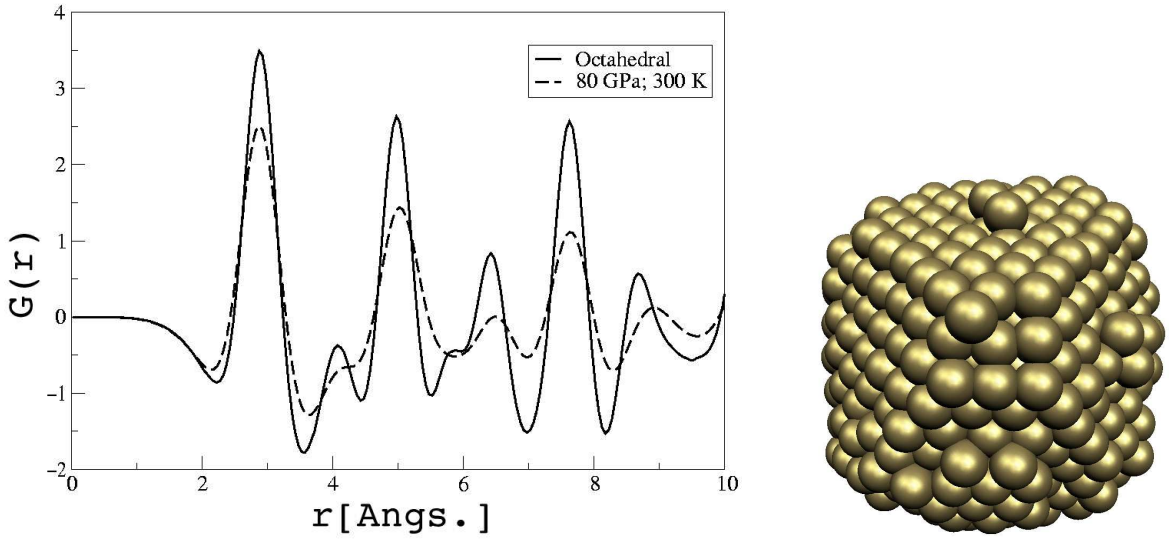

Figure 4.18: (a) RDF of Octahedral under 80 GPa at 300K (670 atoms) with the RDF of Initial configuration. (b) A snapshot of the final octahedral cluster configuration.

Chapter 5

Concluding remarks and future work

5.1 Conclusions

We have analysed several finite systems with different models and approaches. The objective was to obtain reliable methods that could be applied to other finite nanostructures. These methods reveal the existence of new structures that could be metastable under normal conditions and with different mechanical and electrical properties under pressure conditions.

- We have used various methods to apply an external hydrostatic pressure to finite systems. Some of these methods have been reported and others have been introduced and tested in this work. Considering the method of extended Lagrangian, we have found that the volume definition is important in order to have appropriate description of the physical phenomenon.

- The study of a hollow system such as C_{60} under external pressure, using all models and volume definitions, reveals that some definitions like the atomic volume approach is not suitable to study these kind of structures. We have also found, that the classical description of the pressure reservoir and particle interactions has to be carefully considered, in order to avoid the effects produced by non homogeneous liquid systems. This kind of simulation requires an

enormous computational effort so it is restricted to study small finite systems. We have also found that the C_{60} is stable at pressures around 35-40 GPa.

- For single walled nanotubes, we have obtained that the average description of volume is not suitable to study asymmetric systems. The hydrostatic pressure effect could also be studied using the adapted convex volume definition, because it would provided a more precise description of the volume and surface when compared to the volume obtained using the gyration radii. The stability of these nanotubes is found at 5 GPa with no temperature restriction.

- The study of nanodiamonds applying definition III demostrates that an amorphisation process occurs when the pressure is larger than 50 GPa, and it is more pronounced at higher temperatures.

- The study of concentric fullerene-like structures (*Nanonions*) reveals an amorphisation of the structure at 50 GPa. The process associated with this phenomenon, using the volume from gyration radii, could not be precise and the adapted convex volume would be more suitable in this tipe of structure.

- The study of gold clusters demostrates that the volume definition according to the gyration radii allow us to detect structural transitions from octahedral symmetry to a more stable phase with icosahedral symmetry. This transition has been observed, considering a cube octahedral cluster de 561 atom, at 10 GPa of external pressure and 300 K. We have also found that the truncated octahedral shows a change only in its surface, when an external pressure is applied, due to an external pressure is applied, but these changes are not stable when the pressure returns to zero.

5.2 Summary of contributions

- Two suitable methods for studying finite systems under pressure are presented and written in FORTRAN 90 code:
  - The first one uses a volume definition derived from gyration radii to apply in the total coordinates dependence algorithm.
  - Considering an adapted convex volume definition, which allows us to study concave structures. It can be applied on the surface coordinates algorithm.
- Pressure effects on gold clusters have been sstudied using the classical molecular dynamics approach.
- Structural changes on finite SWCNTs caused by external pressures have been observed.

5.3 Future research

We have found that in order to apply an external pressure on finite systems, is important to use an appropriated definition of the volume where the system is enclosed.
In this work, we have analysed two kinds of structures, hollow and compact structures, obtaining that the adapted convex volume definition could be applied to hollow structures.
In the case of the volume obtained from gyration radii definition, it has been shown some applications in compact gold structures.
We will continue this work in the future, and some research directions are:

- Study the effects of external pressure on carbon nanotubes (finite and infinite approach), considering the adapted convex volume definition.
- Study of structural transformation of concentric fullerene systems under pressure in order to find diamond-like structures formation.

- The results obtained in gold clusters show the applicability of the volume definition obtained from the gyration radii to study other metal cluster and alloys.

- We have used a serial program code implemented in FORTRAN 90. The parallelisation of this program would enable us to study larger systems that have an important computational cost using, for example, tight-binding calculations.

Bibliography

[1] O. C. Roemer(1644-1710), D. G. Fahrenheit(1686-1736), R. A. Ferchault de Réamur (1683-1757) and A. Celsius (1701-1744) are some of the scientists that created the first temperature measurements considering boiling (100 celsius degree) and freezing (0 celsius degree) points of water to stablish scales of temperature.

[2] J.D. Bernal, *A geometrical approach to the structure of liquids.* Nature **183** 141-147 (1959)

[3] J.D. Bernal and J. Mason, *Coordination of randomly packed spheres.* Nature **188** 910-911 (1960)

[4] B.J. Alder and T.E. Wanwright, *Phase transition for a hard sphere system.* J. Chem. Phys **27** 1208-1209 (1957)

[5] A.T. Bell, *The Impact of Nanoscience on Heterogeneous Catalysis.* Science **299** 1688-1691 (2003)

[6] S.O. Obare, R.E. Hollowell and C.J. Murphy, *Sensing Strategy for Lithium Ion Based on Gold Nanoparticles.* Langmuir **18** 10407-10410 (2002)

[7] T. Park, Z. A. Dreger and Y. M. Gupta, *Raman Spectroscopy of pentaerythritol Single Crystals under High Pressures*, J. Phys. Chem. B **108** 3174-3184 (2004)

[8] H. C. Andersen, *Molecular dynamics simulations at constant pressure and/or temperature*, J. Chem. Phys **72** 2384. (1980)

[9] M. Parrinello and A. Rahman, *Crystal Structure and Pair Potentials: A Molecular-Dynamics Study* Phys. Rev. Lett. **45** 1196-1199. (1980)

[10] D. Y. Sun and X. G. Gong, *A new constant-pressure molecular dynamics method for finite systems*. J. Phys: Condens. Matter **14** L487-L493. (2002)

[11] A. I. Landau, *A new Method of molecular dynamic computer simulation at constant temperature and pressure*, J. Chem. Phys. **117** 8607-8612.(2002)

[12] D. Y. Sun and X. G. Gong, *Structural properties and glass transition in Al_n clusters*, Phys. Rev. B **57** 4730-4735.(1998)

[13] F. Calvo and J. P. K. Doye, *Pressure effects on the structure of nanostructures*, Phys. Rev. B **69**, 125414. (2004)

[14] R. Martonak, C. Molteni and M. Parrinello, *Ab Initio Molecular Dynamics with a Classical Pressure Reservoir: Simulation of Pressure-Induced Amorphisation in a $Si_{35}H_{36}$ Cluster*,Phys. Rev. Lett. **84** 682-685. (2000)

[15] L.D. Landau and E. Lifshitz,*Statistical Physics*, Pergamon press, Pag. 89 (1974)

[16] J. Tersoff, *New Empirical Model for the Structural Properties of Silicon*, Phys. Rev. Lett. **26** 632.(1986)

[17] S. Maruyama and Y. Yamaguchi *A Molecular Dynamics Demonstration of Annealing to a Perfect C_{60} Structure*, Chem Phy. Letter **286** 343-349.(1998)

[18] Y. Yamaguchi and S. Maruyama, *A Molecular Dynamics simulation of the fullerene formation process*, Chem Phy. Letter **286** 336-342.(1998)

[19] F. Cleri and V. Rosato, *Tigh-binding potential for transition metals and alloys*, Phys. Rev. B **48** 22-33.(1993)

[20] D. Brenner, *Empirical potential for hydrocarbons for use in simulating the chemical vapor deposition of diamond films*, Phys. Rev. B **42** 9458.(1990)

[21] Yi Xiao, F. Patolsky, E. Katz, J. F. Hainfeld and I. Willner, *Plugging into Enzymes: Nanowiring of Redox Enzymes by a Gold Nanoparticle*. Science **299** 1877-1881 (2003)

[22] C. Molteni, R. Martonak and M. Parrinello, *First principles molecular dynamics simulations of pressure-induced structural transformations in silicon clusters*,J. Chem. Phys. **114** 5358-5365.(2001)

[23] W. Hoover, M. Ross and K. Johnson, *Soft-Sphere equation of state*, J. Chem. Phys. **52** 4931-4941.(1993)

[24] R.P.Gupta,*Lattice relaxation at a metal surface*, Phys. Rev. B **23** 6265-6270.(1985)

[25] L. Verlet, *Computer "Experiments" on Classical Fluids. I. Thermodynamical Properties of Lennard-Jones Molecules*, Phys. Rev. **159** 98-103 (1967)

[26] D. Frenkel and B. Smit, *Understanding molecular simulation*, Academic Press Pag. 74 (2002)

[27] D. Brown and J. H. R. Clarke, *A comparison of constant energy, constant temperature and constant pressure ensembles in molecular dynamics simulations of atomic liquids*, Molecular Physics **51** 1243-1252 (1984)

[28] H. W. Kroto, J. R. Heath, S. C. O'Brien, R. F. Curl and R. E. Smalley, C_{60}*: Buckminsterfullerene*,Nature **318** 162-163 (1985)

[29] C. Kittel, *Introduction to Solid State of Physics*. Ed. Wiley,(1996)

[30] C. B. Barber, D.P. Dobkin and H. Huhdanpaa, *The Quickhull algorithm for Convex Hulls*, ACM Transactions on Mathematical Software, **22**, 469-483.(1996)

[31] H. Zabrodsky, S. Peleg and D. Avnir, *Continuos Symmetry Measures. 2. Symmetries Groups and the Tetrahedron*, J. Am. Chem. Soc, **115**, 8278-8289.(1993)

[32] G. Gao, T.Cagin and W. A. Goddard III, *Energetics, structure, mechanical and vibrational properties of single-walled carbon nanotubes*, Nanotechnology **9**, 184-191. (1998)

[33] M. S. Dresselhaus, G. Dresselhaus and P. C. Eklund *Science of Fullerenes and Carbon Nanotubes*, Academic Press (1996)

[34] J. Tang, L. Qin, T. Sasaki,M. Yudasaka, A. Matsushita and S. Iijima, *Compresibility and Poligonization of single-walled carbon nanotubes under hydrostatic pressure*, Phys. Rev. Lett. **85**, 1887. (2000)

[35] J. A. Elliot, J. K.W. Sandler, A. H. Windle, R. Young and M. S. P. Shafter*Collapse of single-walled carbon naotubes is diameter dependent*, Phys. Rev. Lett. **92**, 95501. (2004)

[36] J. Zang, A. Treibergs, Y. Han and F. Liu, *Geometric constant defining shape transitions of carbon nanotubes under pressure*, Phys. Rev. Lett. **92**, 105501. (2004)

[37] S. Iijima and T. Ichihashi, *Structural instability of ultrafine particles of metals*, Phys. Rev. Lett. **56**, 616. (1986)

[38] S. Iijima, *Helical microtubles of graphitic carbon*, Nature **354**, 220-222. (1991)

[39] T.W. Ebbesen and P.M. Ajayan, *Large Scale Synthesis of Carbon Nanotubes*, Nature **358**, 220. (1992)

[40] T. Ichihashi and S. Iijima, *Roles of laser light and heat in formation of single-wall carbon nanotubes by pulsed laser ablation of CxNiyCoy targets at high temperature*. Journal of Physical Chemistry B **102**, 10207 (1998).

[41] B. Zheng, Y. Li, J. Liu, *CVD synthesis and purification of single-walled carbon nanotubes on aerogel-supported catalyst*, Applied Phys. A **74**, 345-348. (2002)

[42] M. Endo, K. Takeuchi, S. Igarashi, K. Kobori, M. Shiraishi and H. W. Kroto*The production and structure of pyrolytic carbon nanotubes (PCNTs)*,J. Phys. Chem. Solids, **54**, 1841 (1993)

[43] F. Banhart,*The transformation of graphitic onions to diamond under electron irradiation*,J. Appl. Phys **81** 3440-3445 (1997)

[44] F. Banhart and P. M. Ajayan, *Carbon onions as nanoscopic pressure cells for diamond formation*, Nature **382** 433-435 (1996)

[45] C. L. Cleveland and U. Landman, *The energetics and structure of nickel clusters: Size dependence*, J. Chem. Phys.**94**, 7376 (1991)

[46] E. L.Nagaev *Equilibrium and quasiequilibrium properties of small particles*, Phys. Rep. **222** 199-307 (1992)

[47] K. Koga and T. Ikeshoji and K. Sugawara, *Size and Temperature-Dependent structural transitions in Gold Nanoparticles*, Phys. Rev. Lett. **92**, 115507. (2004)

[48] K. Koga and K. Sugawara, *Population statistics of gold nanoparticle morphologies: direct determination by HREM observations*, Surface Science. **529**, 23-25. (2003)

[49] D.K.Saha, K. Koga and H. Takeo, *Stable icosahedral nanoparticles in an as-grown Au-Fe alloy*, Eur. Phys. J.D.**9**, 539-542. (1999)

[50] H.S. Nam, N.M. Hwang, B. D. Yu and M. J.-K.Yoon, *formation of an icosahedral cluster during the freezing of gold nanoclusters: surface induces mechanism* Phys. Rev. Lett.**89**, 255502. (2002)

[51] C.L.Cleveland, W.D. Luedtke and U. Landman, *Melting of gold clusters*, Phys. Rev. B **60**, 115507. (1999)

[52] J. T. Frey and D. J. Doren, **TubeGen 3.1** (web-interface, http://deaddog.duch.udel.edu/ frey/research/tubegenonline.html), University of Delaware, Newark DE, (2003).

[53] J. M. Montejano-Carrizales, J.L. Rodríguez-López, C. Gutierrez-Wing, M. Miki-Yoshida, and M. José-Yacamán, *Crystallography and Shape of Nanoparticles and Clusters: Geometrical Analysis, Image and Diffraction Simulation, and High Resolution Images* Encyclopedia of Nanoscience and Nanotechnology, Edited by H. S. Nalwa, (American Scientific Publishers, Los Angeles, 2004), Vol. 2, Cap. 30, pp. 237-282.

[54] K. Sattler, J. Muhlbach, O. Echt, P. Pfau and E. Recknagel, *Evidence for Coulomb Explosion of Doubly charged microclusters*, Phys. Rev. Lett. **47** 160-163 (1981)

[55] T. P. Martin, *Shells of atoms* Phys. Rep. **273**,199 (1996).

[56] C.C. Chen, A.B.Herhold,C.S. Johnson and A.P.Alivisatos *Size dependence of structural metastability in semiconductor nanocrystals*, Science **276** 398-401 (1997)

[57] R. G. Osifchin, R. P. Andres, J. I Henderson, C. P. Kubiak and R. N Dominey,*Synthesis of nanoscale arrays of coupled metal dots*,Nanotechnology **7** 412-416 (1996)

[58] Karvat A, Duzenli C, Ma R, et al ,*The treatment of choroidal melanoma with 198 Au plaque brachytherapy*,Radiother Oncol **59** 153-6, (2001)

[59] J.F. Hainfelf, and R.D. Powell,*New frontiers in gold labeling*J. Histochem. Cytochem. **48** 471-480 (2000)

[60] T. L. Daulton, D. D. Eisenhour, T. J. Bernatowicz, R. S. Lewis and P. R. Buseck, *Genesis of presolar diamonds: comparative high-resolution transmission electron microscopy study of meteoritic and terrestrial nanodiamonds* Geochim. Cosmochim. Acta **60** 4853-4872 (1996)

[61] There are several kinds of RDF for amorphous carbon (at different densities). In this case, the curve of an amorphous phase was obtained using the software Cerius 2. Reference: Molecular Simulations Inc., Cerius2 Modeling Environment, Release 4.0, San Diego: Molecular Simulations Inc., 1999.

[62] G. E. Tommei, F. Baletto, R. Ferrando, R. Spadacini, and A. Danani, *Energetics of fcc and decahedral nanowires of Ag, Cu, Ni, and C[60]: A quenched molecular dynamics study*, Phys. Rev. B **69**, 115426 (2004)

[63] J. L. Rodríguez-López, F. Aguilera-Granja, K. Michaelian, and A. Vega, *Structure and magnetism of cobalt clusters*, Phys. Rev. B **67**, 174413 (2003)

[64] W. Y. Choi, J. W. Kang, and H. J. Hwang, *Structures of ultrathin copper nanowires encapsulated in carbon nanotubes*, Phys. Rev. B **68**, 193405 (2003)

Appendix A

Study on Noncrystalline Solids

We know that is very difficult to identify a kind of structure when we are considering liquid, glass, disordered, amorphous or non-periodic systems.
In this situation, we can still extract some information. For example, we could obtain information from diffraction patterns that can be obtained using X-ray or neutron scattering. In both cases, we normally obtain diffuse rings on the normal incident plane. This also ocurrs when the system has a small size so we obtain again a diffuse pattern similar to an amorphous system. Instead of study this pattern, we can also obtain the main structural order (for example, the distance at first neighbors).
Using a Fourier analysis of the experimental X-ray scattering curves, it is possible to obtain a more specific information: **The radial distribution function**. This could be applied to liquids, glasses, or a powdered crystalline material.

A.1 RDF

If we are considering a non-periodic system, we must express the structure factor in its general expression:

$$S(\Delta\mathbf{k}) = \sum_m f_m e^{i\Delta\mathbf{k}\cdot\mathbf{r}_m} \tag{A.1}$$

where the sum runs over all atoms in the system, so Δk are arbitrary scattering vectors, and f_m is the atomic form factor. The scattered instensity at scattering vectors is expressed by:

$$I = S^*S = \sum_m \sum_n f_m f_n e^{i\Delta\mathbf{k}\cdot(\mathbf{r}_m - \mathbf{r}_n)} \tag{A.2}$$

Taking the spherical average of the exponential term due to isotropic symmetry and if we consider a monoatomic system ($f_m = f_n = f$):

$$I = Nf^2\Big[1 + \sum_m{}' \frac{\sin Kr_{mn}}{Kr_{mn}}\Big] \tag{A.3}$$

where the sum runs over all atoms m with the exception of $m = n$ case. After that, we can obtain the intensity using the concentration of atoms $\rho(r)$ at distance r from a reference atom and integrating until a large radius R:

$$I = Nf^2\Big[1 + \int_0^R dr 4\pi r^2 \rho(r) \frac{\sin Kr}{Kr}\Big] \tag{A.4}$$

If we consider an average concentration ρ_0, we could separate this effect (scattering from a uniform concentration) and rewrite this expression as:

$$I = Nf^2\Big[1 + \int_0^R dr 4\pi r^2 [\rho(r) - \rho_0] \frac{\sin Kr}{Kr} + \frac{\rho_0}{K}\int_0^R dr 4\pi r \sin Kr\Big] \tag{A.5}$$

the second term may be neglected when $R \to \infty$(except for small angles).

The structure factor from a liquid monoatomic system can be defined now as

$$S(k) = \frac{I}{Nf^2} \tag{A.6}$$

and if we neglect the uniform concentration effect,

$$S(k) = 1 + \int_0^\infty dr 4\pi r^2 [\rho(r) - \rho_0] \frac{\sin Kr}{Kr} \tag{A.7}$$

at this point we define the **radial distribution function** $g(r)$ as

$$g(r) = \frac{\rho(r)}{\rho_0} \tag{A.8}$$

so this function is a spherically averaged distribution of interatomic distances(this is also called *two-atom correlation function*). Sometimes, the function plotted is the reduced function $G(r)$ that is defined by

$$G(r) = 4\pi r \rho_0 (g(r) - 1) \tag{A.9}$$

Also we can use again the spherical symmetry to write $S(K)$ as a Fourier integral of a function of g(r) and viceversa using the Fourier integral theorem.

Appendix B

Point Groups

A point group is a group of symmetry operations which leaves at least one point unmoved. In this context, groups are classified by their symmetry operations. These operations could be: identity, rotation respect of an axis, reflection in a plane of symmetry, inversion and improper rotation.
Using this operations, molecules are classified in one of several **point groups**, and this notation is called *Schoenflies system*. The symmetry in molecules can be organized as follows:

1. The groups C_s,C_i,C_1: systems that have only a plane of symmetry apart from Identity.

2. The groups C_n: in this case n-fold axis of symmetry are possible (+ Identity).

3. The groups C_{nv}: structures that have a C_n axis and n vertical reflection planes σ_v (+ Identity).

4. The groups C_{nh}: These groups consider a C_n axis and a perpendicular horizontal mirror plane .

5. The groups D_n: molecules that possess a C_n axis and n 2-fold axes that are perpendicular to C_n.

6. The groups D_{nh}: Objects that belong to D_n and consider a horizontal mirror plane.

7. The groups D_{nd}: Objects that belong to D_n and consider vertical mirror planes bisecting angles between all the neighbouring C_2 axes.

8. The cubic groups T, O and their derivatives: sistems that have more than one principal axis of symmetry. We have to consider the tetrahedral groups T, T_d and Th and the octahedral groups O and O_h.

9. The Icosahedral groups: these molecules contain Icosahedral and dodecahedral symmetries.

10. The full rotation group R_3: this systems have the group of operations shown by a spherical object.

The crystal symmetry is also classified and is given by the *Hermann-Mauguin system.* If we want to consider translational periodicity, some point groups, like Icosehedrals, are discarded and the new summary containing 32 groups is:

Type	Symbol
Non Axial	C_i, C_s
Cyclic	C_1, C_2, C_3, C_4, C_6
Cyclic with horizontal planes	C_{2h}, C_{3h}, C_{4h}, C_{6h}
Cyclic with vertical planes	C_{2v}, C_{3v}, C_{4v}, C_{6v}
Dihedral	D_2, D_3, D_4, D_6
Dihedral with horizontal planes	D_{2h}, D_{3h}, D_{4h}, D_{6h}
Dihedral with planes between axes	D_{2d}, D_{3d}
Improper Rotation	S_4, S_6
Cubic Groups	T, T_d, T_h, O, O_h

Figure B.1: Crystallographic point groups.